UNIVERSITI PENDIDIKAN SULTAN IDRIS
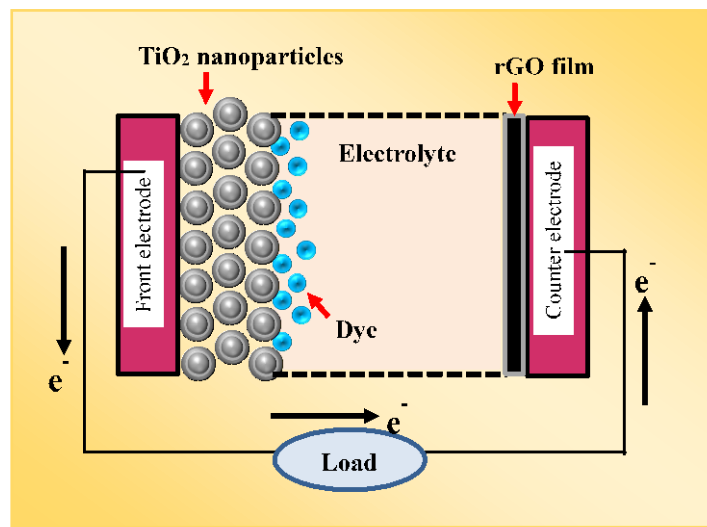اونيۏرسيتي ڤنديديقن سلطان ادريس
SULTAN IDRIS EDUCATION UNIVERSITY

TEACHING INOVASION:

SIMPLE DEVELOPMENT OF SOLAR CELL
(*DYE-SENSITIZED SOLAR CELLS*)
TEACHING AID FOR ENERGY PHYSICS-SFG3033


ASSOC. PROF. DR. SURIANI ABU BAKAR

DEPARTMENT OF PHYSICS
FACULTY OF SCIENCE AND MATHEMATICS

TABLE OF CONTENT

As an alternative renewable energy, solar energy has been extensively developed to slowly replace conventional energy sources, such as fossil fuels. Solar cells are considered an important device to convert solar energy to electricity power directly. In solar cell groups, dye-sensitized solar cells (DSSC) have been widely explored owing to the advantages, such as reasonable conversion efficiency, simple fabrication, low-cost, weak toxicity, flexibility, and light weight [1].
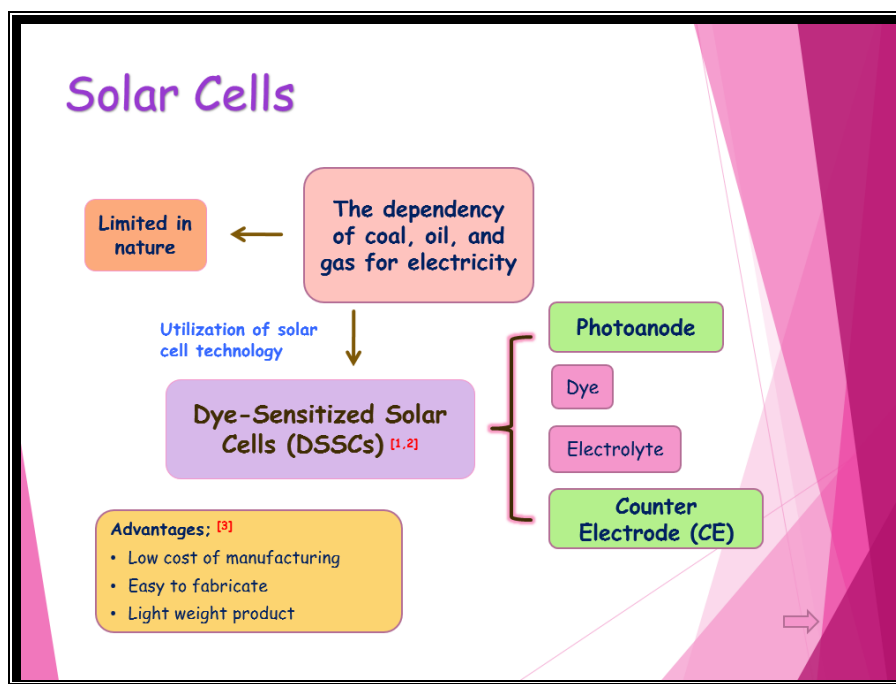
The DSSC comprise three <u>main components</u>:

   i.   **a transparent conductive glass as a photoanode (titanium dioxide, zinc oxide and tin oxide),**
   ii.   **a catalytic counter electrode (CE) as a cathode (platinum (Pt) or carbon)**
   iii. **a redox couple as an electrolyte (trioxide/iodide) [2] (see Figure 1 and 2)**
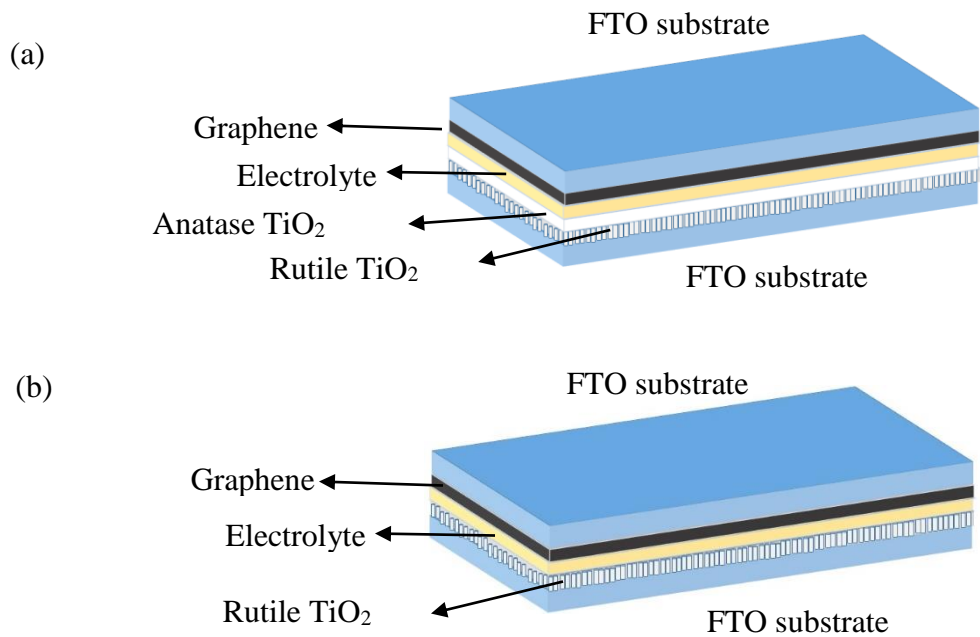
Figure 1. Illustration of different configurations of TiO$_2$ nanostructured-graphene electrodes (a) Rutile/anatase-graphene and (b) rutile-graphene.
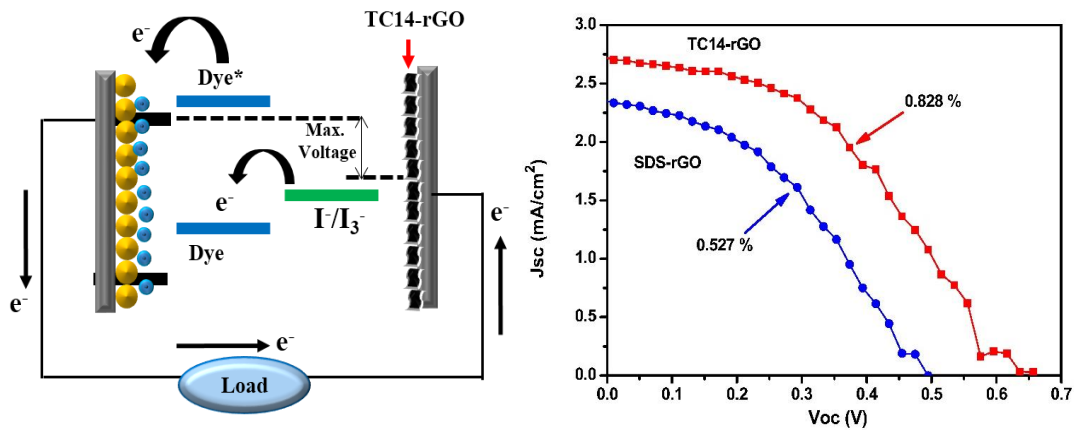
Figure 2. Schematic of DSSC assembled sample and J-V curve of DSSC.

A CE is an important component to regenerate a photosensitizer or dye, after an electron is injected; this component can then act rapidly to reduce the overall potential. The Pt-based CE in DSSC has also been introduced because of its high catalytic activity and chemical stability toward I$^-$/I$_3^-$ electrolyte [1, 3]. However, with high costs of Pt (~$1456 per Troy ounce at present) [3], tremendous effort have

4

been taken to develop cost-effective CEs for DSSC and thus reduce the fabrication cost of device [4–6].

Carbon-based materials, such as carbon nanotubes (CNTs), are established as a CE materials for the photovoltaic enhancement in DSSC (Figure 3). Synthesized CNTs usually retain defect sites that act as an extra electron for kinetic transfer [7] rarely caused by functionalization and treatment processes [8]. These defects are also necessary to improve the DSSC performance. However, a complex technology should be developed because of costly and limited CNTs production.
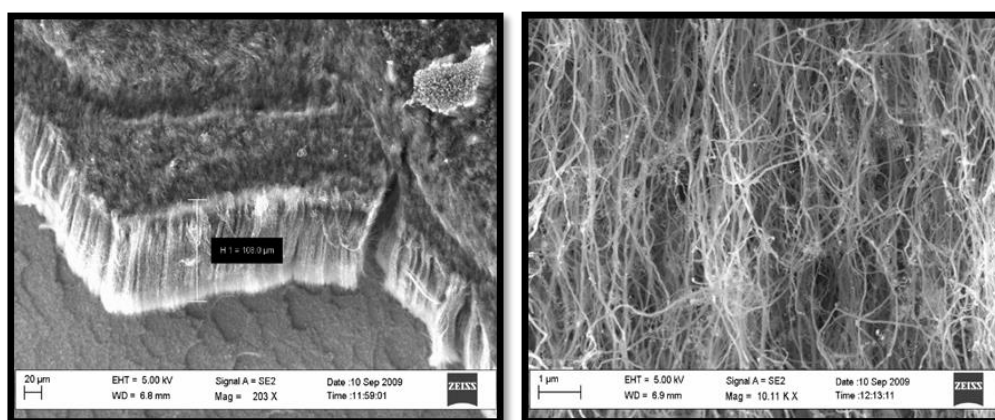
Figure 3. CNTs are established as a CE materials for the photovoltaic enhancement in DSSC.

New carbon materials, graphene has excellent properties such as low charge transfer resistance, high surface-to-volume ratio, high chemical resistance, high carrier mobility, and high catalytic activity, which are suitable for the high performance and long-term stability of DSSC [1, 9, 10]. A two-dimensional honeycomb lattice material, graphene is considered as a potential candidate for Pt-free CE for DSSC.

GRAPHENE

➢ **Graphene**: consists of one atom thick layer which built up from **six-neighbours of carbon** arranged in a **hexagonal lattice**

➢ The calculated adjacent carbon atoms length and interlayer spacing between sheets are **1.41 Å** and **3.35 Å**, respectively

➢ Discovered by **Novoselov- 2004**
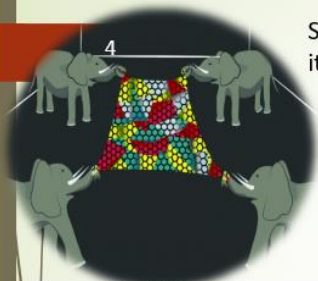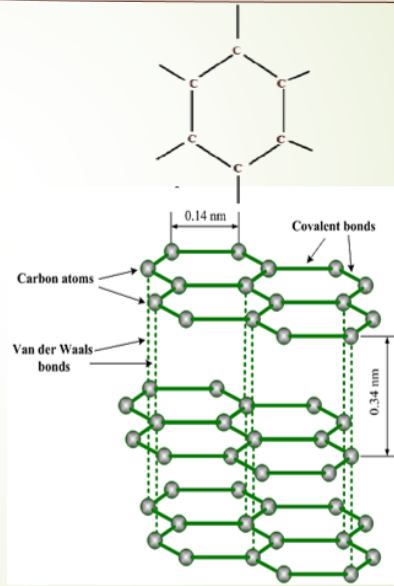
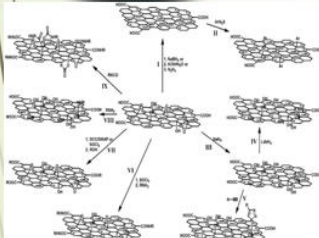
Strectable up to 20% of its initial length

Why graphene?

Harder than diamond 300x harder than steel

Can be functionalized by several chemical groups (for instances OH-, F-) forming graphene oxide and fluorinated graphene

Great conductor -electrons travel carry no mass, as fast as just 100x that of the speed of light.

Thinnest material ever made

Graphene is synthesized by using top-to-down or bottom-to-up approaches that offer low-cost production. Solution-processing methods, such as electrochemical exfoliation, are more favourable than chemical vapour deposition because the former can be used for green and scalable production of single and multiple graphene layers in dispersions at low temperatures [8]. The functionalization and hybridization of graphene can be easily altered through solution-based approaches because functionalized graphene can provide more active sites for electron transfer kinetics in photovoltaic studies.
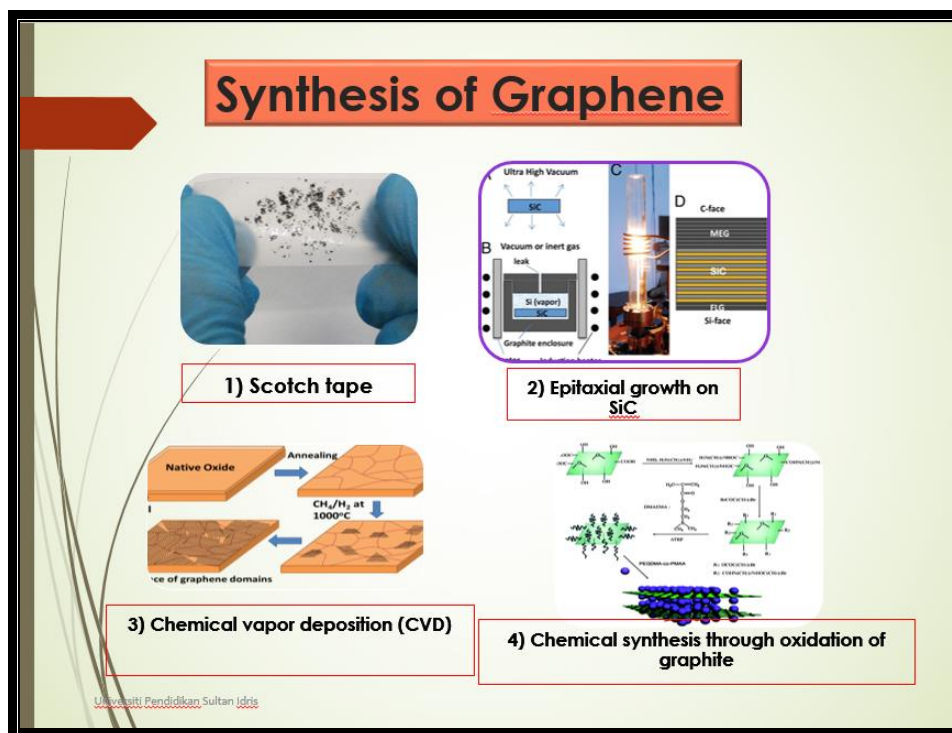
A calculated efficiency of approximately 2.8% is obtained for graphene -based materials as CE in DSSC [12]. In addition, photovoltaic measurements have been greatly enhanced after reduction of GO into rGO by using various amounts of hydrazine as reducing agents [13]. This phenomenon confirms that the density of introduced defects generates more active sites on the surface of reduced graphene oxide (rGO) based CE thus enhanced the DSSC performance [14]. Xu et al. also demonstrated the important role of other impurities or groups, such as NCHO in the functionalized rGO; as a result, its catalytic activity is higher than that of pristine graphene and rGO [15]. They found that oxygen-containing functional groups in graphene can enhance the catalytic performance of a DSSC device because edge sites promote a faster electron movement than basal sites do [16]. Thus, suitable synthesis methods for graphene production should be selected to

maintain the catalytic performance percentage of oxygen-containing groups. The GO is reduced to rGO through chemical reduction, and this process is favourable because of its controllable production, convenience, and rapid reaction that can result in a massive amount of rGO in dispersions [17]. A surfactant is utilized as a stabilizer to stabilize rGO sheets in an aqueous solution because of a high van der Waals interaction between graphitic structures.

Among various CE fabrication methods, spraying (Figure 4) has been mostly investigated because of its portability, simplicity, and flexibility on various large-area substrates; in contrast to spraying, sputtering and dip coating methods require ultra-high vacuum facilities and thus entail costly DSSC applications [18].
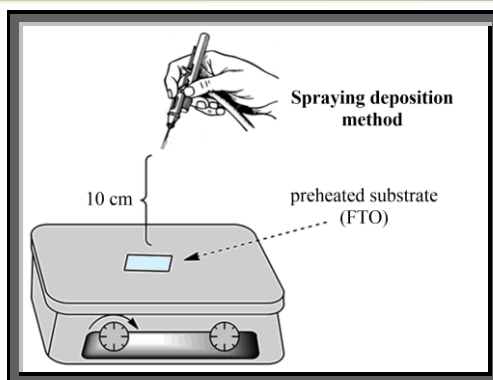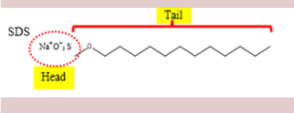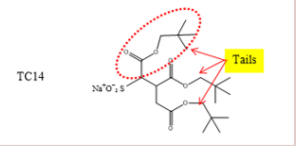
Figure 4. Transfer process of graphene using spray deposition method

The effectiveness of using a custom-made triple-chain surfactant, namely, 1,4-bis(neopentyloxy)-3-(neopentyloxycarbonyl)-1,4-dioxobutane-2-silphonate (TC14), as a good stabilizer of GO/rGO and natural rubber latex (NRL) has been described [19]. This surfactant provides triple interactions and helps prevent GO/rGO agglomerations in dispersion. In contrast to commercially available sodium dodecyl sulphate (SDS), TC14 allows high interactions between GOrGO and NRL matrix; as a result, the stability of GO/rGO is increased [20].

In this study, TC14 and SDS surfactant are used to improve the stability of rGO sheets. GO is initially synthesized through electrochemical exfoliation by utilizing both surfactants and then subjected to chemical reduction by using hydrazine hydrate at a ratio of 100:1. The effects of the surfactants are systematically evaluated on the basis of the properties of rGO-based CE and the performance in DSSC. The results revealed that the proposed simple rGO film preparation can be applied to produce low-cost CE with a high energy conversion efficiency for DSSC.
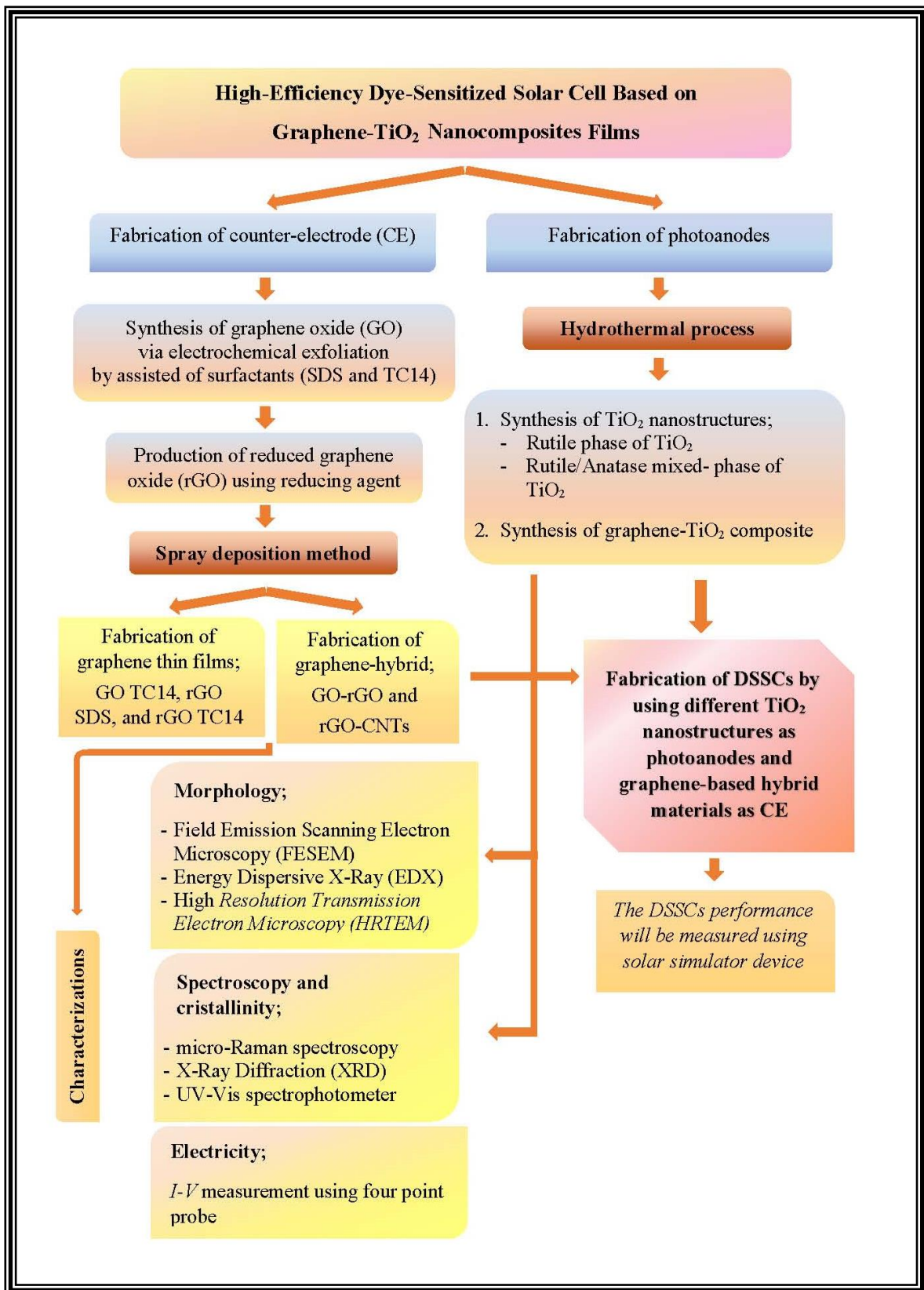
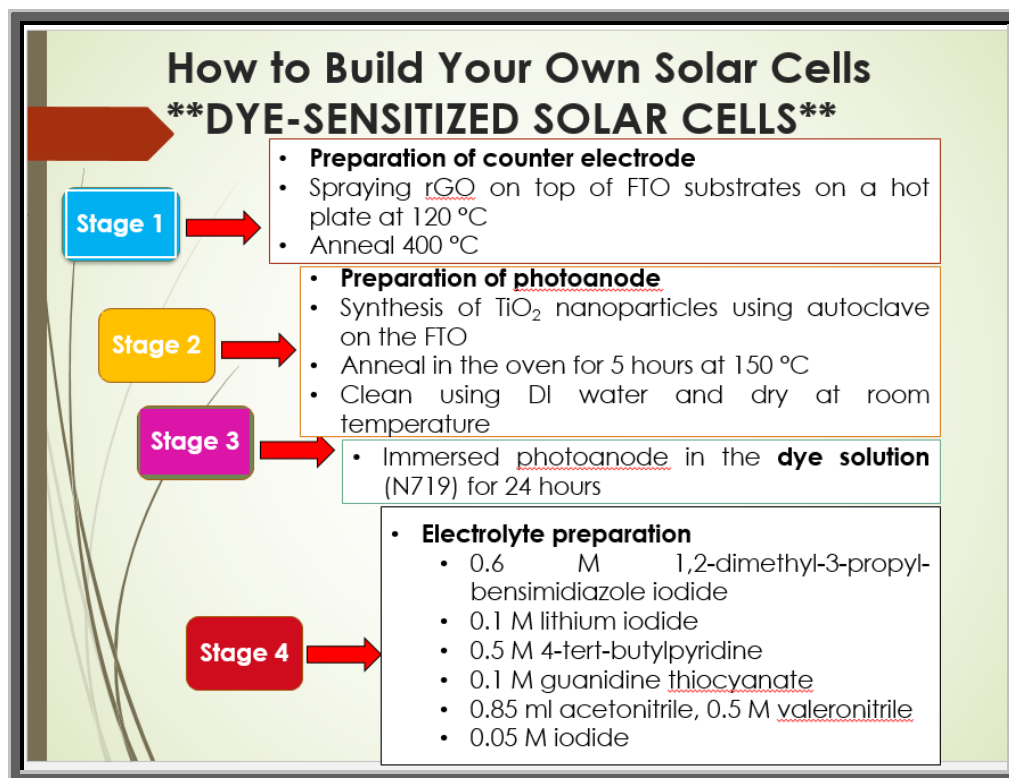Figure 5. The flow chart of the methodology to build the solar cells.

Chemicals

In the production of graphene, two pieces of high purity graphite rods (99.99 %) (GoodFellow GmbH, Germany), with a diameter and length of 10 and 150 mm, respectively, are used in the electrochemical exfoliation method.

For the synthesis of TC14 surfactant, the chemicals used including neopentyl alcohol (Acros Organics, 50g), trans-aconitic acid (Sigma Aldrich, 100g), toluene-4-sulfonic acid monohydrate (Merck, 1 kg), toluene (Merck, 17 L), silica gel (Acros Organics, 5 kg), diethyl ether (Chem AR, 2.5 L), petroleum ether 40-60 (Merck, 17 L), alugram sheets (Macherey Nagel, 1 box), ethanol (Merck, 25 L), sodium bisulfite (Friendemann Schmidt, 1 kg) and methanol (Merck, 25 L).

Meanwhile, hydrazine hydrate (Merck, 80 % soluble in water) is used as a reducing agent. Fluorine-doped tin oxide (FTO)-coated glass substrate (Sigma-Aldrich) is used as substrates. The TiO_2 photoanode is prepared by mixing of 0.3 g of powder anatase TiO_2 (d = 25 nm), acetic acid and liquid anatase TiO_2 (d = 6 nm).

The dye used is N719 purchased from Sigma Aldrich. Dimethyl-propyl-benzimidiazole iodide (DPMII) electrolyte was prepared from 0.6 M 1,2-dimethyl-3-propyl-benzimidiazole iodide (Sigma-Aldrich), 0.1 M lithium iodide (Sigma-Aldrich), 0.5 M 4-tert-butylpyridine (Sigma-Aldrich), 0.1 M guanidine thiocyanate (QreC), 0.85 ml of acetonitrile (Sigma-Aldrich), 0.5 ml of valeronitrile (Sigma-Aldrich), and 0.05 M iodide (Sigma-Aldrich).

How to Build Your Own Solar Cells
DYE-SENSITIZED SOLAR CELLS

Stage 1
- **Preparation of counter electrode**
- Spraying rGO on top of FTO substrates on a hot plate at 120 °C
- Anneal 400 °C

Stage 2
- **Preparation of photoanode**
- Synthesis of TiO_2 nanoparticles using autoclave on the FTO
- Anneal in the oven for 5 hours at 150 °C
- Clean using DI water and dry at room temperature

Stage 3
- Immersed photoanode in the **dye solution** (N719) for 24 hours

Stage 4
- **Electrolyte preparation**
  - 0.6 M 1,2-dimethyl-3-propyl-bensimidiazole iodide
  - 0.1 M lithium iodide
  - 0.5 M 4-tert-butylpyridine
  - 0.1 M guanidine thiocyanate
  - 0.85 ml acetonitrile, 0.5 M valeronitrile
  - 0.05 M iodide

Electrochemical Exfoliation Method

Figure 6 shows a schematic diagram of the electrochemical exfoliation method. Two pieces of high purity graphite rods (99.99 %) purchased from Good Fellow Company, Germany, with a diameter and length of 10 and 150 mm, respectively, were used in this study. The experimental setup was done at room temperature. The two graphite rods were connected to the power supply as an anode and cathode electrodes (see Figure 6 & 7). Then, the graphite rods were partially immersed in the electrolyte solution. The electrolyte used was a mixture of dissolved surfactant in deionized water varying in concentration from 0.001 to 1.0 M. A direct current (DC) voltage was applied between the graphite electrodes. The electrochemical exfoliation process that lasted 6 to 48 hours. The exfoliation of bulk graphite into the single sheet occurred in the presence of surfactant intercalated between the interlayer of graphite, as illustrated in Figure 8.
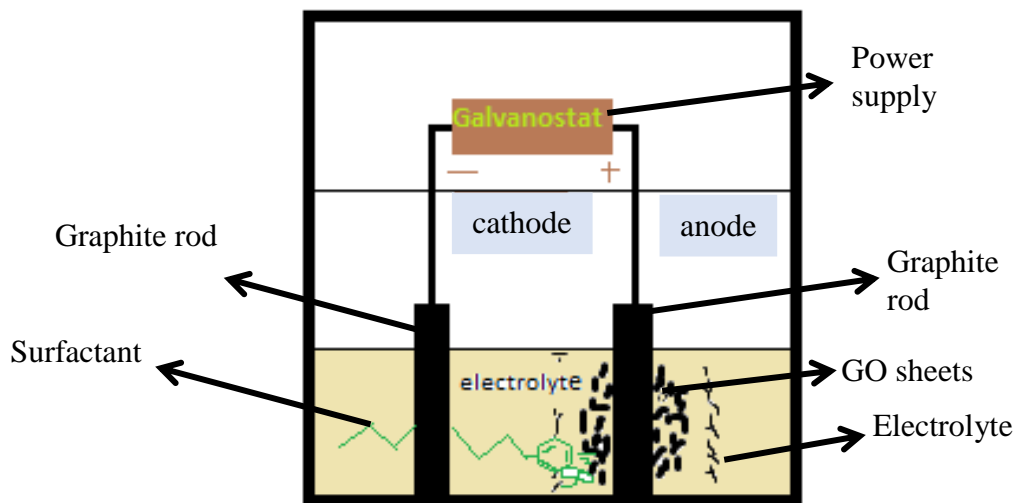
Figure 6. Schematic diagram of the experimental setup for the electrochemical exfoliation method.
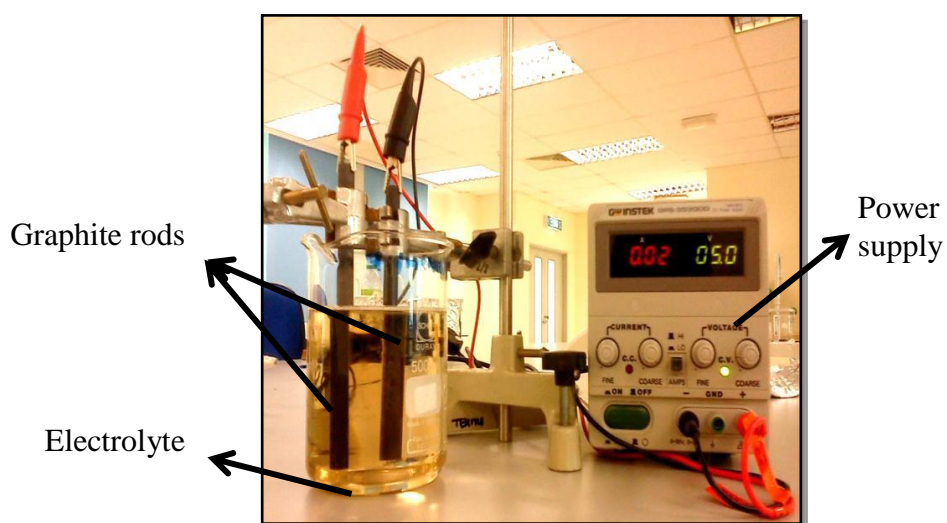
Figure 7. Experimental setup for the electrochemical exfoliation method.

Figure 8. GO production and the presence of surfactant intercalated between the interlayer spacing of graphite layers.

Preparation of reduced graphene oxide

The produced GO solution was further reduced to by using hydrazine hydrate at a volume ratio of 1:100 (hydrazine: GO) at 100 °C for 24 *h*. Detailed preparation procedures of the two-step approach were described as follows (see Figure 9):

Reduction of GO to rGO

I. Hydrazine hydrate (80 % soluble in water) was used as a reducing agent.
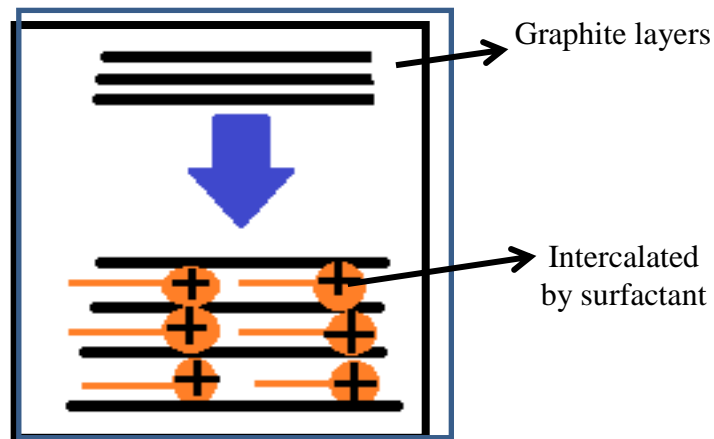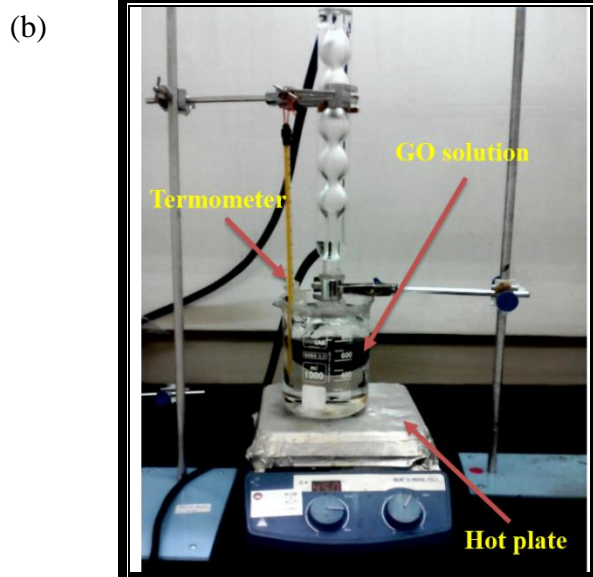
II. First, 1:100 volume ratio of hydrazine hydrate to GO solution was mixed in a triple neck, round bottom flask which was readily immersed in a hot water.

III. The mixture was stirred for 24 hours using a magnetic stirrer at a temperature of around ~100 °C.

IV. Then, the dispersions were subjected to ultrasonic dissolution for 30 minutes.

(a)

(b)
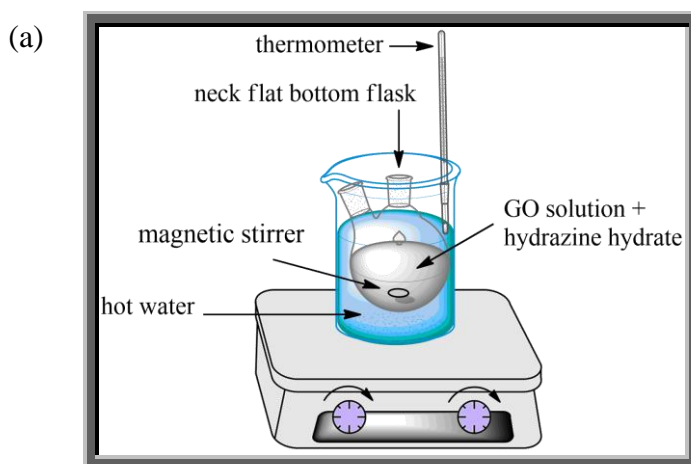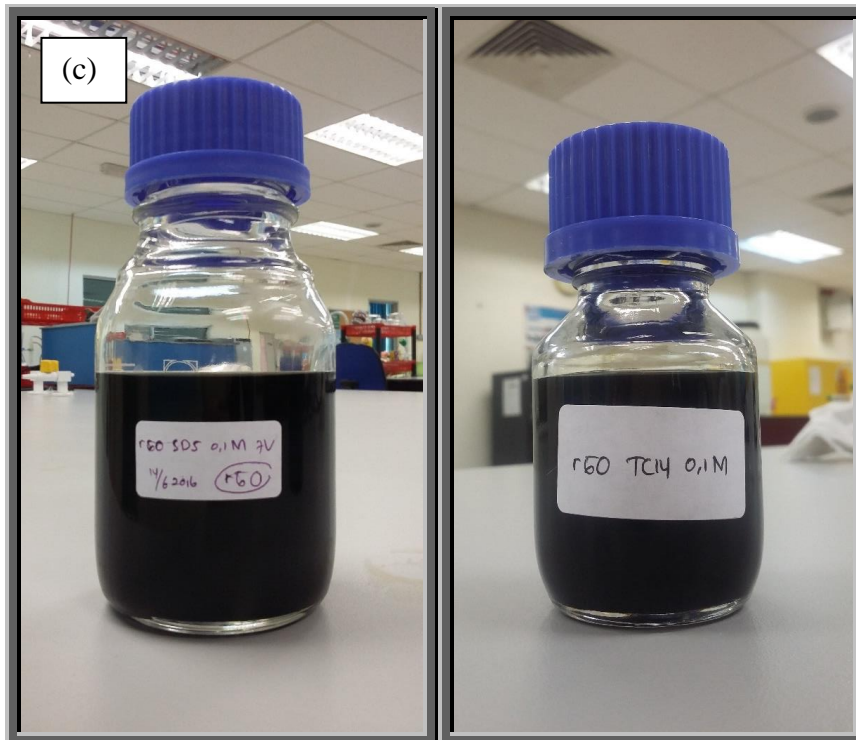
Figure 9. Reduction process using hydrazine hydrate as reducing agent (a) the schematic and (b) typical process done in this study (c) the production of rgo

Spray Coating Method

The transfer process of graphene was done using a simple spray coating method. The samples then annealed into TCVD furnace in argon (Ar) ambient. The schematic diagram and typical spray deposition method with TCVD furnace is shown in Figure 10.

GO synthesis

graphite rod

Electrochemical exfoliation was done at 7V for 24 hours

electrolyte solution containing surfactant

Reduction process

thermometer

magnetic stirrer

hot water

GO solution + hydrazine hydrate

neck flat bottom flask

Fabrication of Graphene thin films

Spray deposition method

10 cm

preheated substrate (FTO)
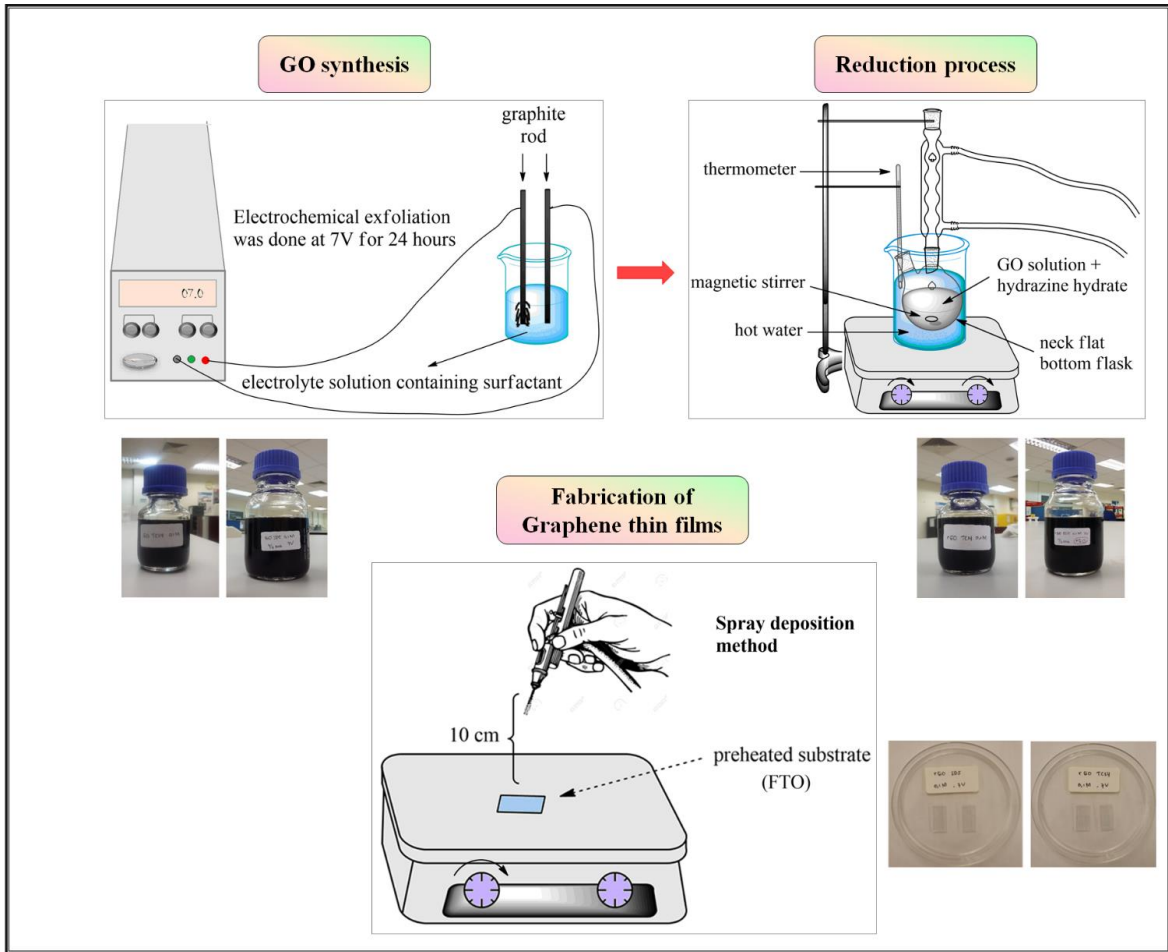
Figure 10. Experimental design of graphene thin film fabrication and the student doing transfer process of graphene using spray deposition method.

Fabrication of Dye-Sensitized Solar Cells

DSSC were fabricated by using a TiO_2-coated FTO glass as a photoanode and an rGO-coated FTO as a CE. In this work, the photoanode with an area of 0.25 cm^2 was sensitized by immersing in N719 dye for 24 h (Figure 11). The sandwich type DSSC was assembled by introducing the liquid electrolyte on the dye-sensitized TiO_2 film and then TC14-rGO counter electrode was clipped firmly with the photoanode and then used to study the photovoltaic performance.

DSSCs fabrication

N719 dye

photoanode

TiO₂ photoanode was immersed in
0.3 mM N719 dye for 24 hours

Dye was prepared by dissolving
N719 dye powder into acetonitrile
and 1-butanol (1:1, v/v)

TiO2 nanostructures

dye

electrolyte

graphene

Synthesis of TiO₂ nanostructured

Pure Rutile

Rutile-anatase mixed-phase
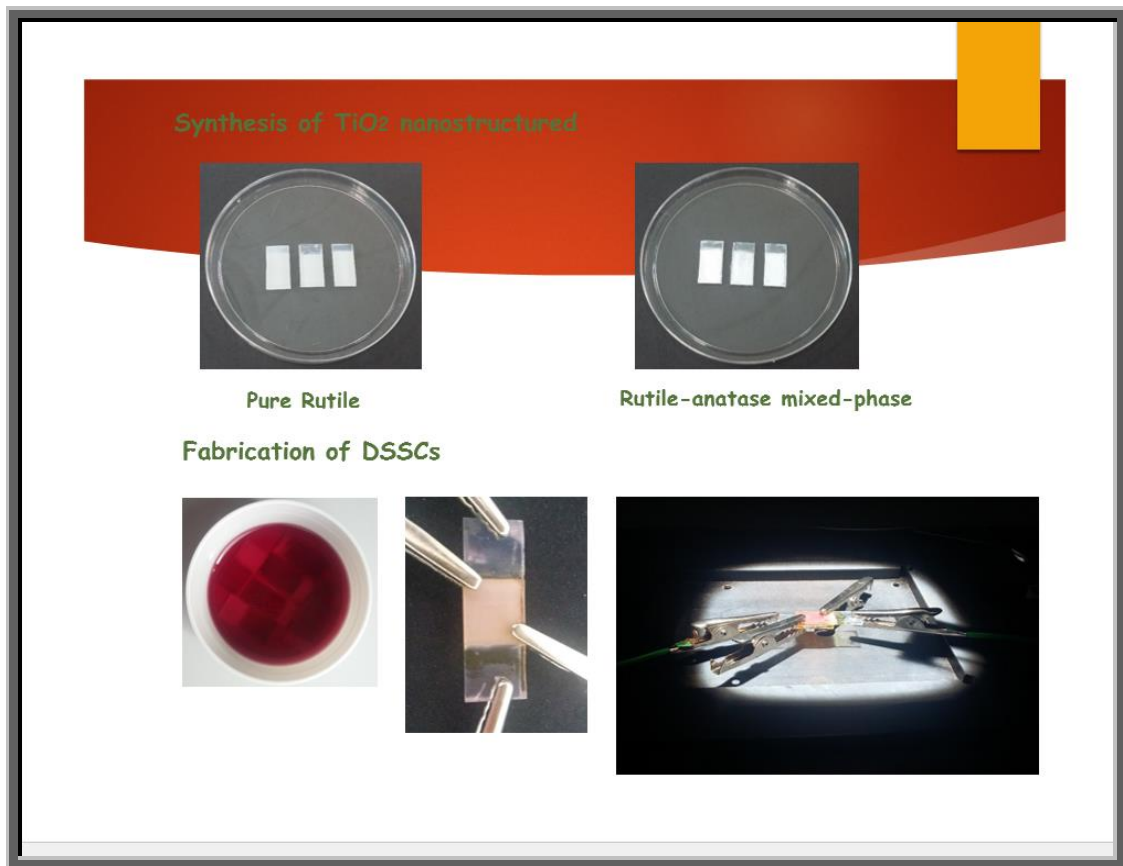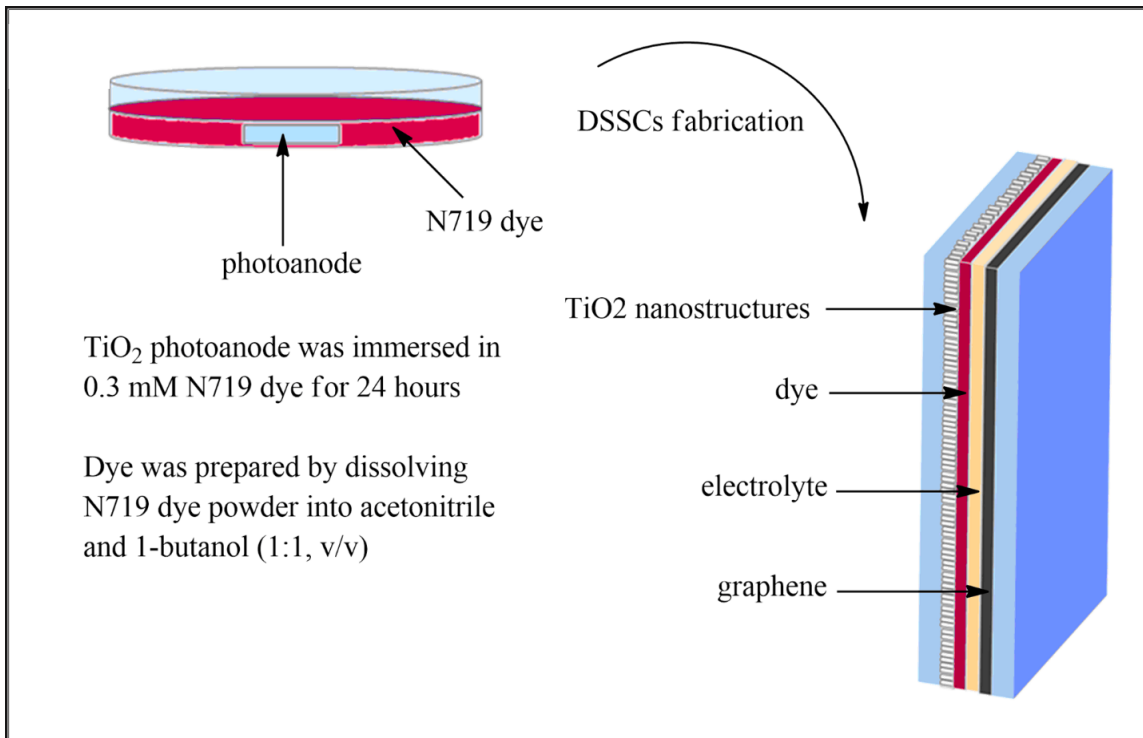
Fabrication of DSSCs

Figure 11. The fabrication of DSSC

Two main steps were involved in the fabrication of TiO_2 photoanode which were (i) preparation of TiO_2 solution and (ii) deposition of TiO_2 thin film (iii) hydrothermal growth of rutile TiO_2 nanorods (iv) squeegee method of TiO_2 nanoparticles. Step (i)-(ii) are for TiO_2 nanoparticles meanwhile step (iii)-(iv) are for hybrid phase of TiO_2.

The details preparation procedures were described as followed:

(i)   Preparation of TiO_2 solution

   I. First, the TiO_2 photoanode was prepared by mixing of 0.3 g of powder anatase TiO_2 (d = 25 nm), acetic acid and liquid anatase TiO_2 (d = 6 nm).
  II. The mixed solution was grinded in the mortar for 10 minutes. After that, the solution was poured inside a bottle. Then, 5 drops of Triton X-100 added with 30 ml of ethanol inside the bottle.
 III. Lastly, the bottle containing solution was placed inside the ultrasonic for 30 minutes.

(ii)   Deposition of TiO_2 thin film

   I. The glass substrates were wrapped with aluminium foil with 0.25 cm^2 hole for masking purpose.
  II. The substrates were placed on the hot plate with temperature of 150 °C.
 III. The TiO_2 solution then was deposited using the spray pyrolysis deposition technique.
 IV. After that, the sample was heated at 150 °C continued with annealing process at 450 °C for 1 hour in the furnace.
  V. The electrolyte then inserted in between the dye-coated photoanode and counter electrode for DSSCs measurement. The schematic diagram of assembled sample for DSSCs measurement is shown in Figure 3.16.
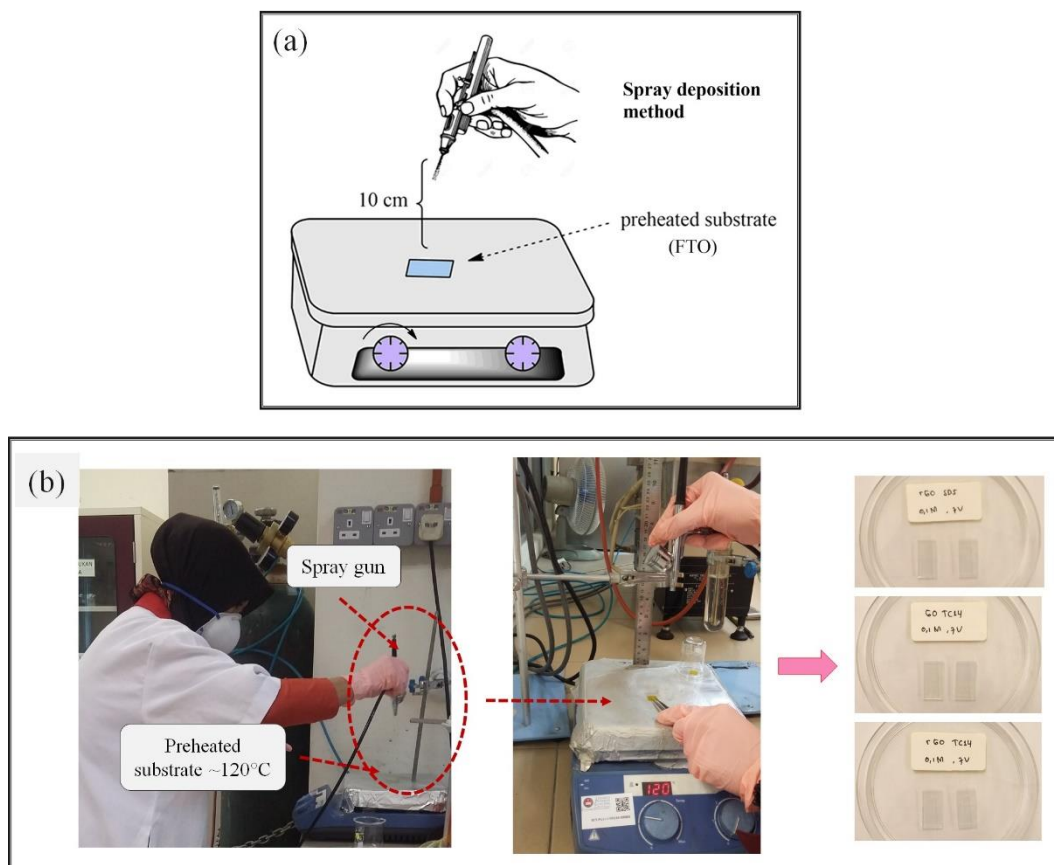
Figure 11. (a) and (b) Deposition of TiO$_2$ thin film

(iii) Hydrothermal growth of rutile TiO$_2$ nanorods

The synthesis of rutile phase TiO$_2$ nanorods was carried out using hydrothermal growth. Hydrochloric acid (HCl) and deionize (DI) water in 1:1 ratio was mixed well before adding titanium butoxide (TBOT) in 1:40 ratio drop by drop to the solution. The solution then stirred for another 10 minutes until mixed. The obtained solution was transferred into an autoclave which had previously been placed FTO substrate with the conducting surface facing upward. The hydrothermal synthesis then carried out at 150℃ for 5 hours. Finally, the synthesized TiO$_2$ was taken out after the autoclave was cooled down into room temperature then rinsed using DI water followed with drying in room temperature. The experimental design of hydrothermal growth process is presented in Figure 12.

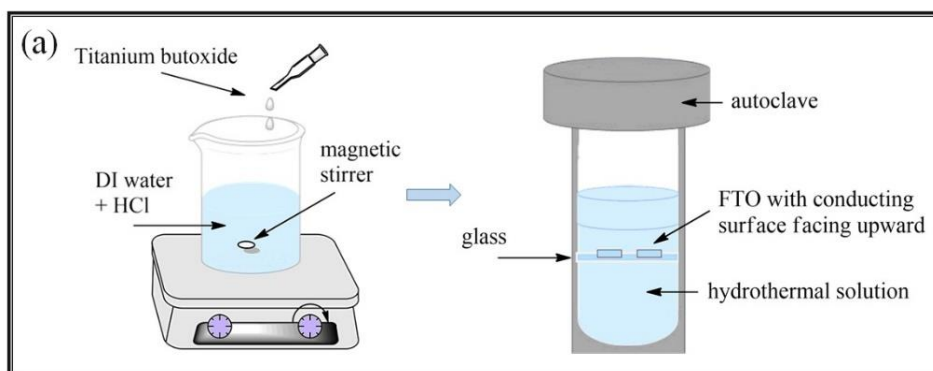(a) Titanium butoxide

DI water + HCl

magnetic stirrer

glass

autoclave

FTO with conducting surface facing upward

hydrothermal solution

Figure 12. (a) The schematic diagram and (b) experimental procedures to synthesize rutile TiO$_2$ nanorods.

(iv) Squeegee method of TiO$_2$ nanoparticles

The TiO$_2$ paste was made by mixing TiO$_2$ P25 DeGussa, ethanol, and titanium (IV) isopropoxide (TTIP). The prepared TiO$_2$ paste was applied on top of rutile TiO$_2$ nanorods film by squeegee method. The mixed-phase TiO$_2$ film then heated on electric oven at 150°C for 10 minutes followed by annealing at 450°C for 1 hour in furnace.
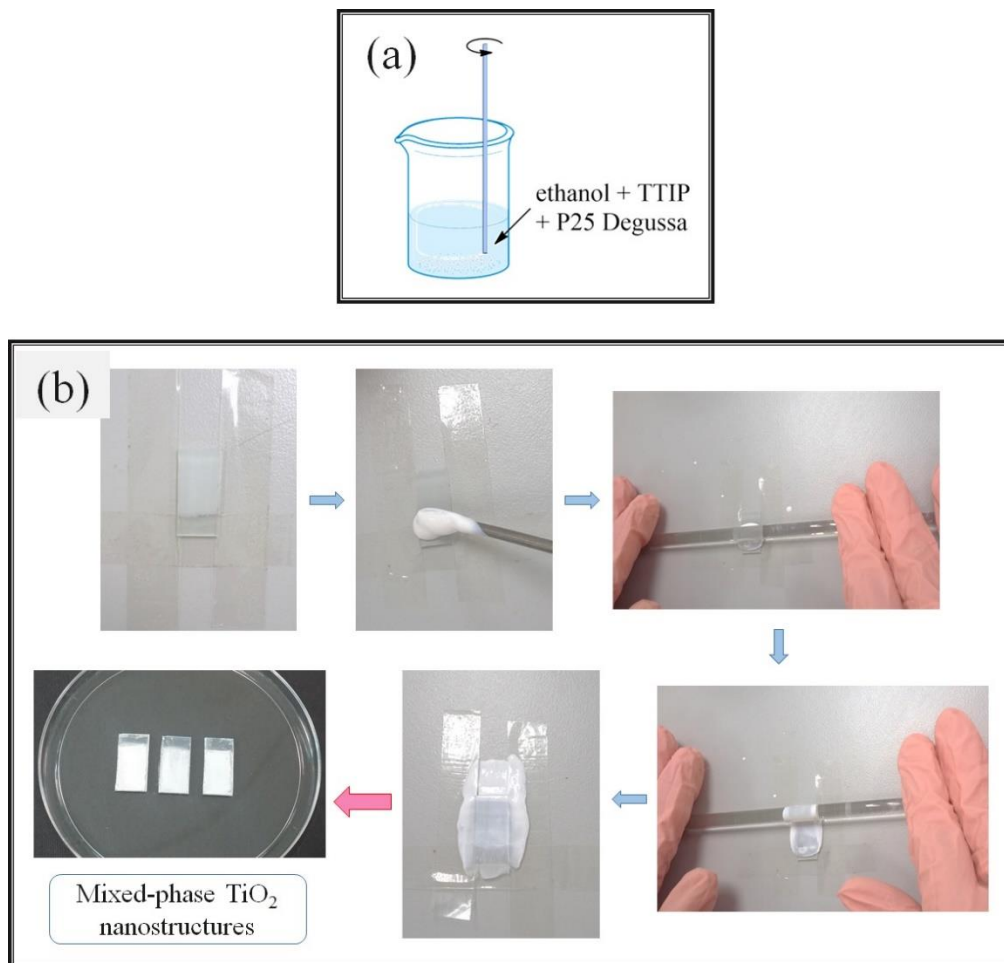

Figure 12 (a) and (b) Squeegee method of TiO$_2$ nanoparticles

Characterization Techniques

The morphology of as-prepared samples were analyzed through field emission scanning electron microscopy (FESEM, Hitachi SU8020). and high-resolution transmission electron microscopy (HRTEM, FEI Tecnai F30). The spectral properites of the samples were accessed using MicroRaman spectroscopy

(Renishaw InVia Raman Microscope), and UV–vis absorption spectroscopy (Agilent 8453 Spectrophotometer) and and Atomic Force Microscope (AFM-X100). The electrical properties were measured using a standard four-point probe instrument. Photovoltaic performance of the fabricated DSSC were evaluated by using a computer-programmed Keithley 2611 Source Meter under the illumination of simulated sunlight (100 mW cm^{-2}, AM 1.5) and a solar simulator (Oriel, 91160-100091192, Parccell Technologies) was used as a light source (see Figure 13-19).
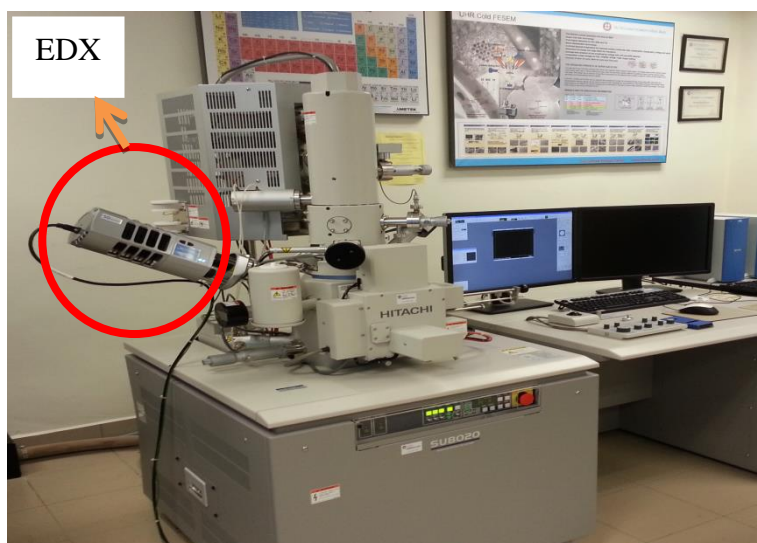

Figure 13. FESEM (Hitachi SU8020) and EDX instrument used to investigate the morphology of as-prepared samples and elemental composition analysis.
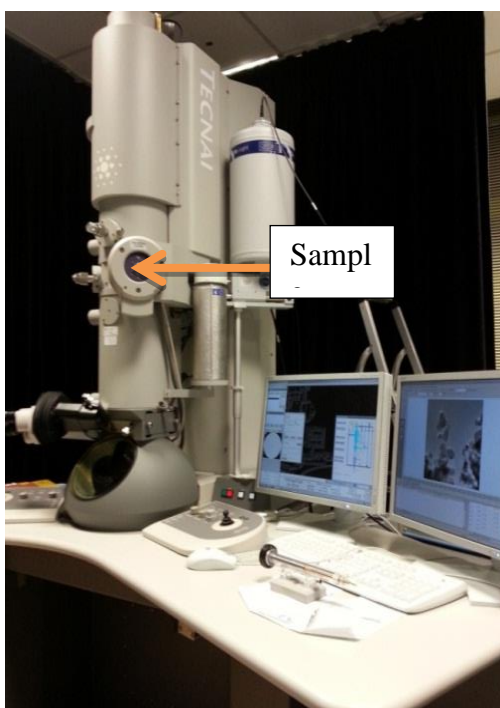
Figure 14. TEM (FEI Tecnai F30) used to investigate the morphology of as-prepared samples.
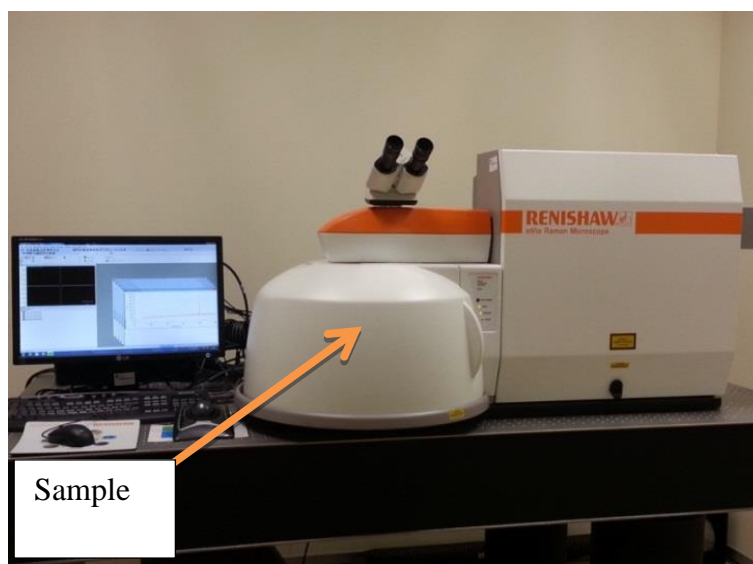
Figure 15. Micro-Raman spectrometer (Renishaw InVia microRaman System) used to investigate the crystallinity of as-prepared samples.

Figure 16. UV-Vis (Agilent Technologies 8453) spectroscopy used to investigate the absorption of GO samples.

Figure 17. AFM measurement of the thickness GO dispersed in ethanol.

Figure 18*. I-V* measurement used to investigate the electrical properties of as-prepared samples.
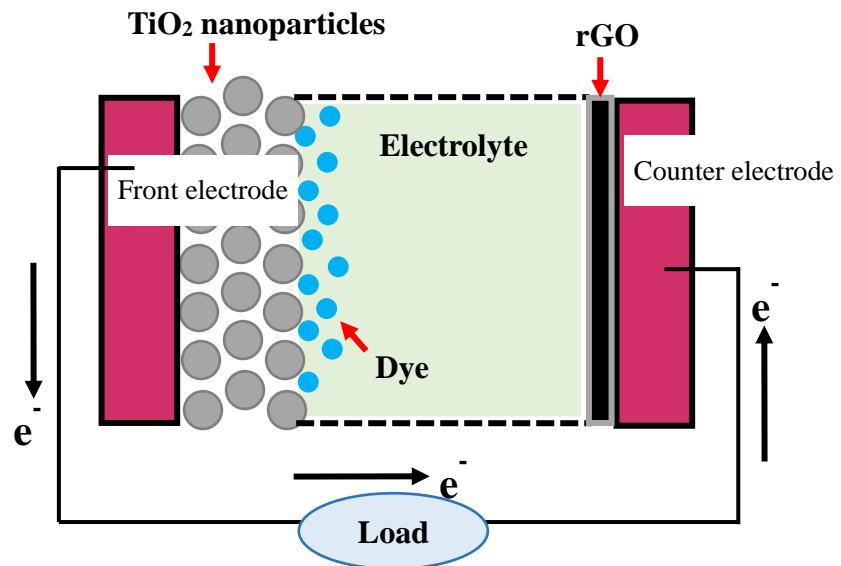
Figure 19. Schematic of DSSCs assembled sample.

3.   Finding and Discussion

Figure 20 (a–f) show the FESEM images of the TC14-rGO, TC14-GO, and SDS-rGO film samples. The FESEM micrographs in Figure 20 (a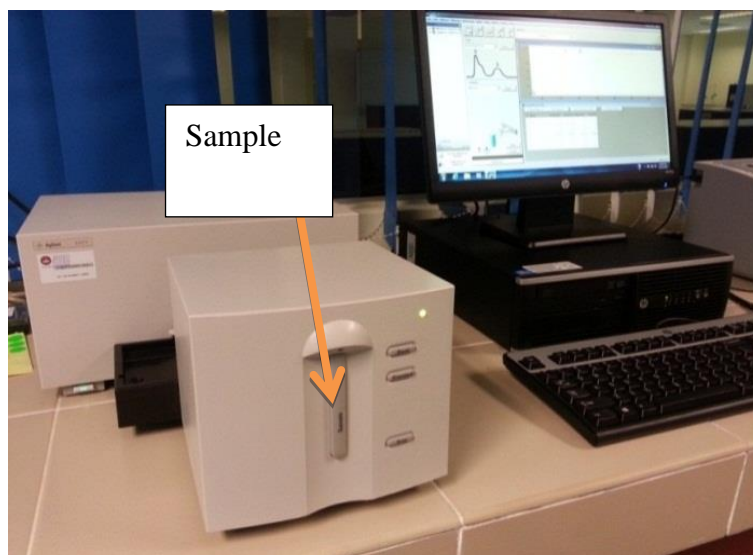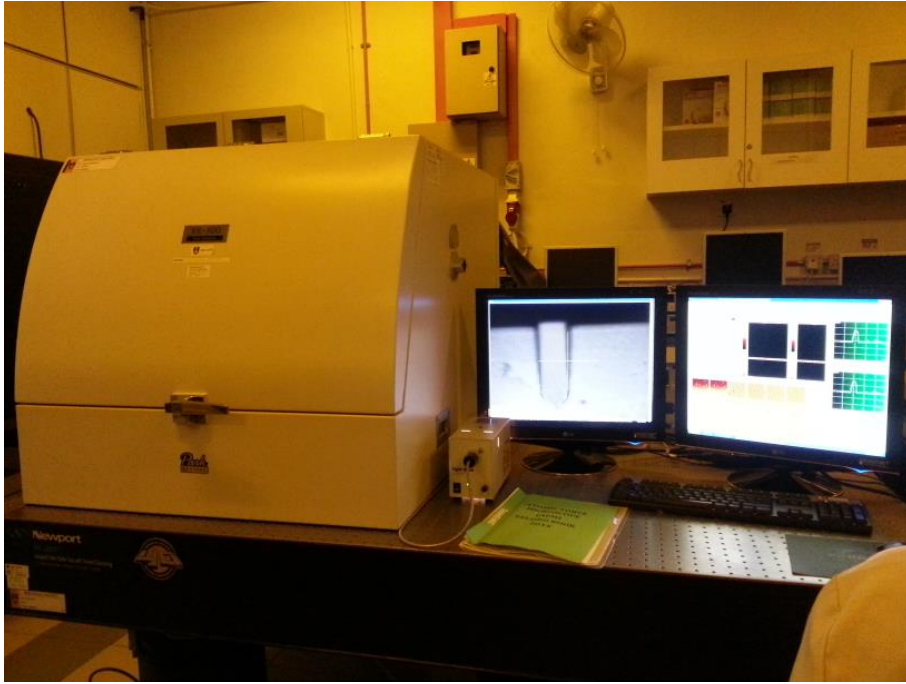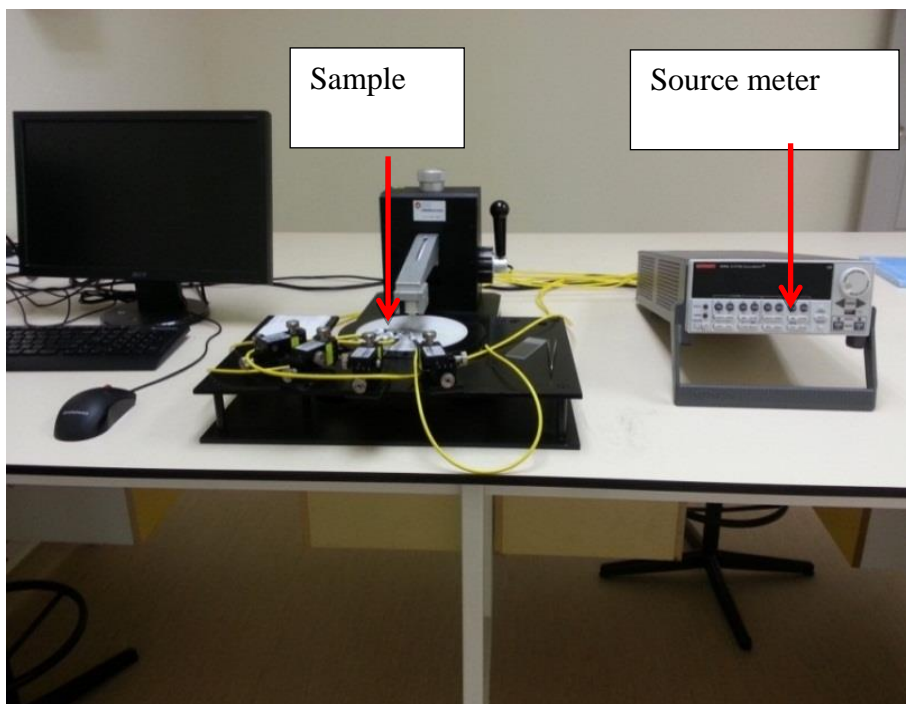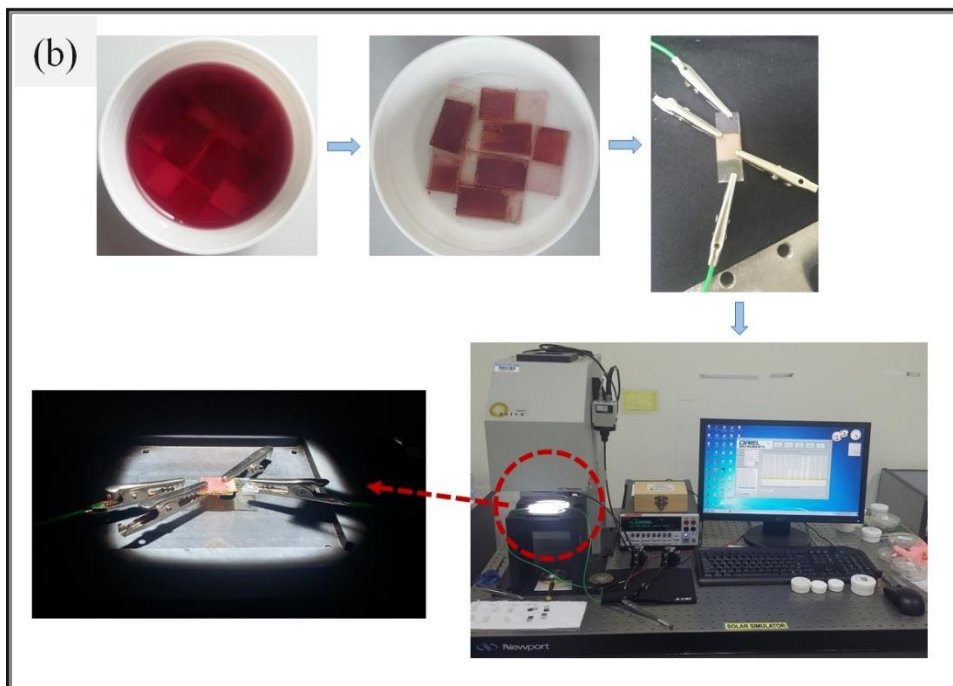-b) reveal that the TC14-rGO sample is composed of large rGO sheets on the FTO glass. A transparent and wrinkled morphology is observed at the edge site (pointed by arrows). This observation is due to the isolated oxygen reaction sites, and the resultant defects are reduced during the chemical reduction of GO [20]. By comparison, the SDS-rGO sample (Figure 20 (c–d)) contains thicker sheets with slightly agglomerated rGO sheets than the other samples do. The uniformity of the TC14-rGO film is retained because of the formation of a well-dispersed and stable solution of rGO assisted by TC14. Compared with those in the TC14-GO sample (Figure 20 (e–f)), the graphitic structures are more densely pack with highly crumpled structures formed through oxidation. As previously reported, the distinct morphologies of the rGO sheets greatly influence the optical and photovoltaic performances [21, 22]. The FESEM images are supported by the findings of HRTEM analysis.
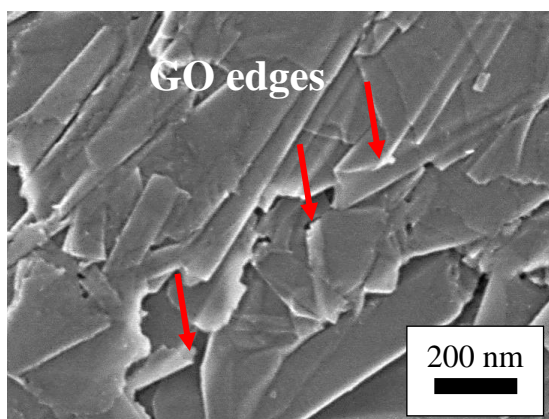
(a) 0.1 M TC14-rGO (50 K X) (b) 0.1 M TC14-rGO (100 K X)

GO edges

200 nm

100 nm
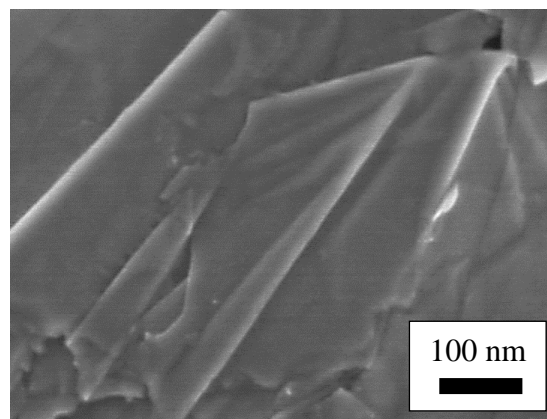
(c) 0.1 M SDS-rGO (50 K X) (d) 0.1 M SDS-rGO (100 K X)

Thick GO

200 nm

100 nm
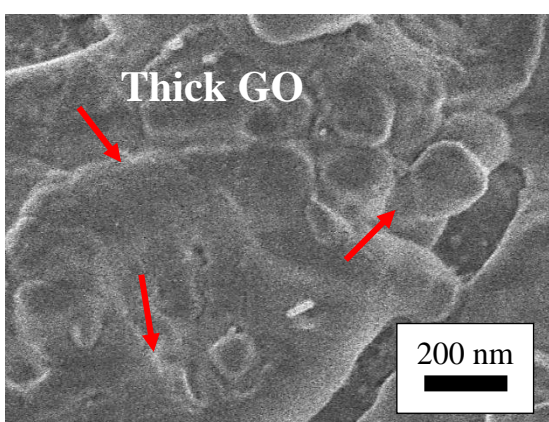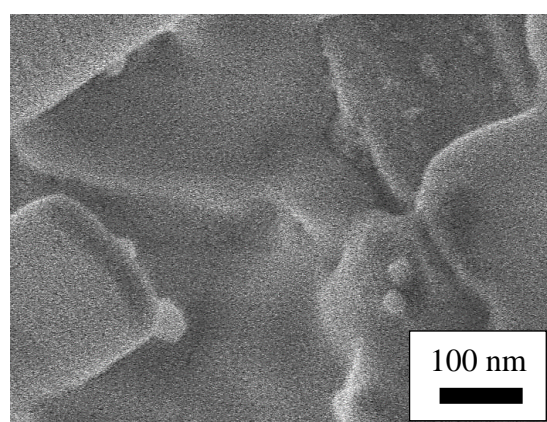
(e) 0.1 M TC14-GO (50 K X) (f) 0.1 M TC14-GO (100 K X)

Wrinkles GO

200 nm

100 nm
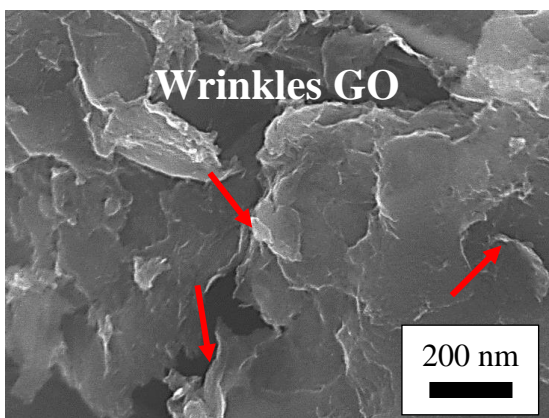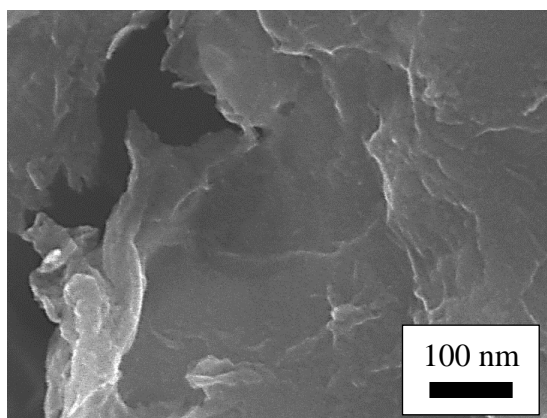
Figure 20. FESEM images of (a)-(b) TC14-rGO, (c)-(d) SDS-rGO and (e)-(f) TC14-GO sheets.

The HRTEM images (Figure 21(a–b)) reveal few rGO layers with large and transparent sheets observed in the TC14-rGO sample, which consists of approximately 2–4 layers. By comparison, the slightly blur image of the TC14-GO sample shows multilayer sheets at the edge site, and these sheets are formed through the insertion of various oxygen-containing functional groups during oxidation (Figure 21 (c)).Significant damages and slightly thick graphitic sheets are

observed in the SDS-rGO sample (Figure 21 (d–e)). The intrinsic wrinkles are found in the calculated layers of approximately 5–6 layers of rGO. These findings indicate that the TC14-assisted rGO possesses a more stable wide-open rGO sheets, which may enhance the diffusibility of electrolytes in DSSC [17, 18, 23, 24]. However, both rGO film samples do not alter the overall morphology of the graphitic sheets.
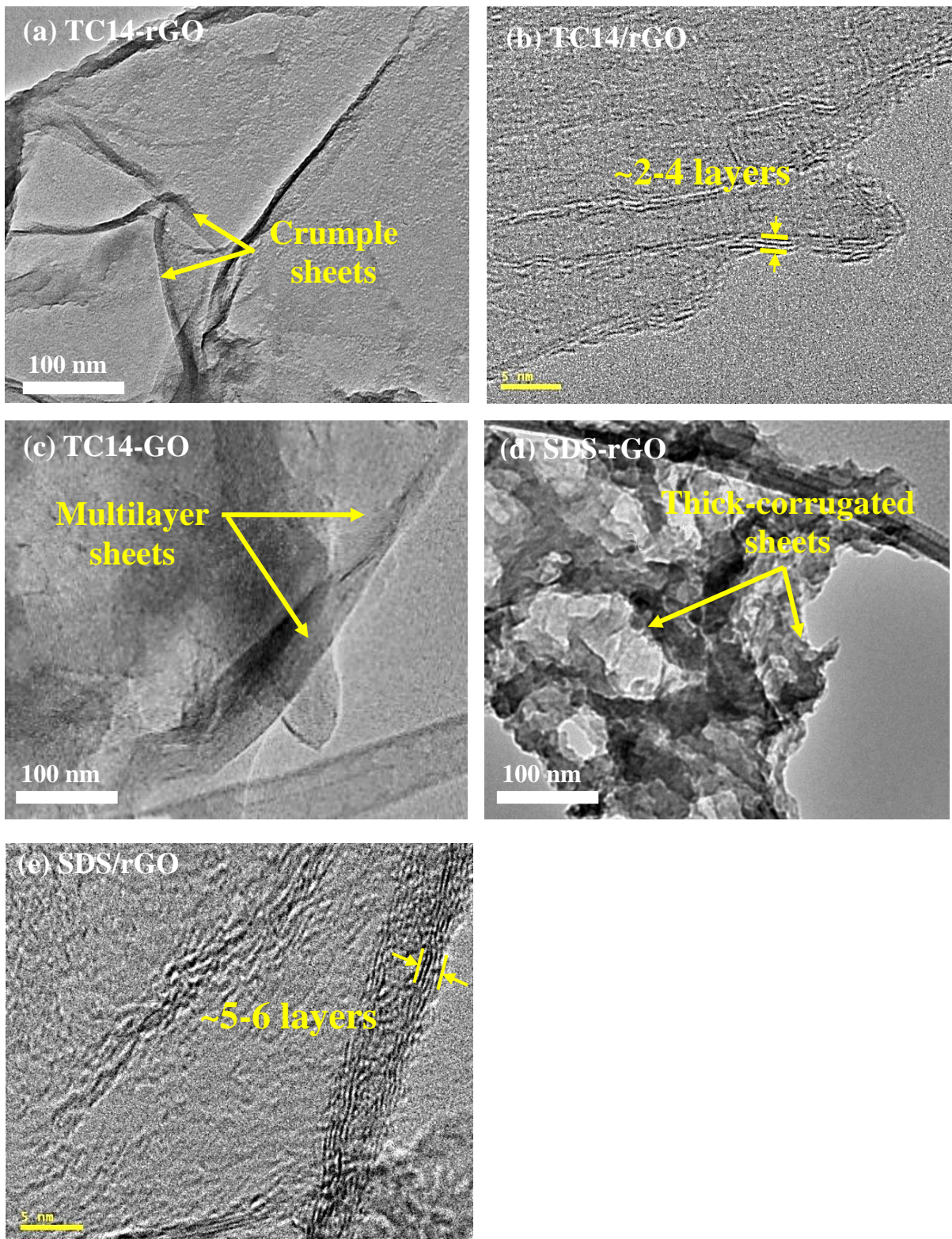
Figure 21. HRTEM images of (a)-(b) TC14-rGO, (c) TC14-GO (d)-(e) SDS-rGO sheets.

The surface morphology of TiO$_2$ nanorods grown on fluorine-doped tin oxide (FTO) substrate is shown in Figure 22 (a). The successfully hydrothermal growth in TiO$_2$ nanorods synthesis is indicated by the dense and uniform nanorods film in the entire FTO surface. The top and closer view of TiO$_2$ nanorods are shown in Figure 22 (b) and (c), respectively. The top view of TiO$_2$ nanorods shows the tetragonal crystal structure with several diameter range of 75.3 to 295 nm as shown in Figure 22 (d). A group of nanoflowers were also observed on the top of nanorods, with complete and uncomplete formed structure as shown in Figure 22 (e). The rarely amount of nanoflowers were caused by the lack time on hydrothermal growth synthesis. Meanwhile, the cross section of the film shows a high-density TiO$_2$ nanorods with the average length of 5.38 μm as shown in Figure 22 (f). The TiO$_2$ nanorods also observed grows nearly perpendicular of FTO surface.

Meanwhile, the surface morphology of TiO$_2$ nanoparticles applied on top of TiO$_2$ nanorods is shown in Figure 22 (g). Based on FESEM images, it can be shown that TiO$_2$ nanoparticles were uniformly and completely covers the nanorods without any cracks. The average diameter of synthesized TiO$_2$ nanoparticles varies from 15.9 to 25.8 nm as shown in Figure 22 (h), which are matches with the average size of P25 Degussa particle. The nanocrystalline particles of TiO$_2$ are linked each other, shows the effectiveness of TTIP's utilization. TTIP will coagulate at each nanocrystalline particles grain boundaries thus makes them completely interconnected.
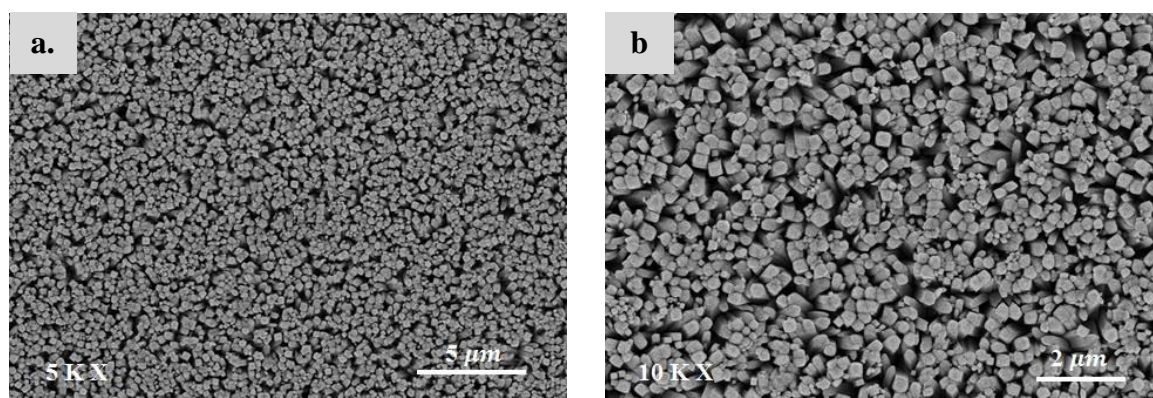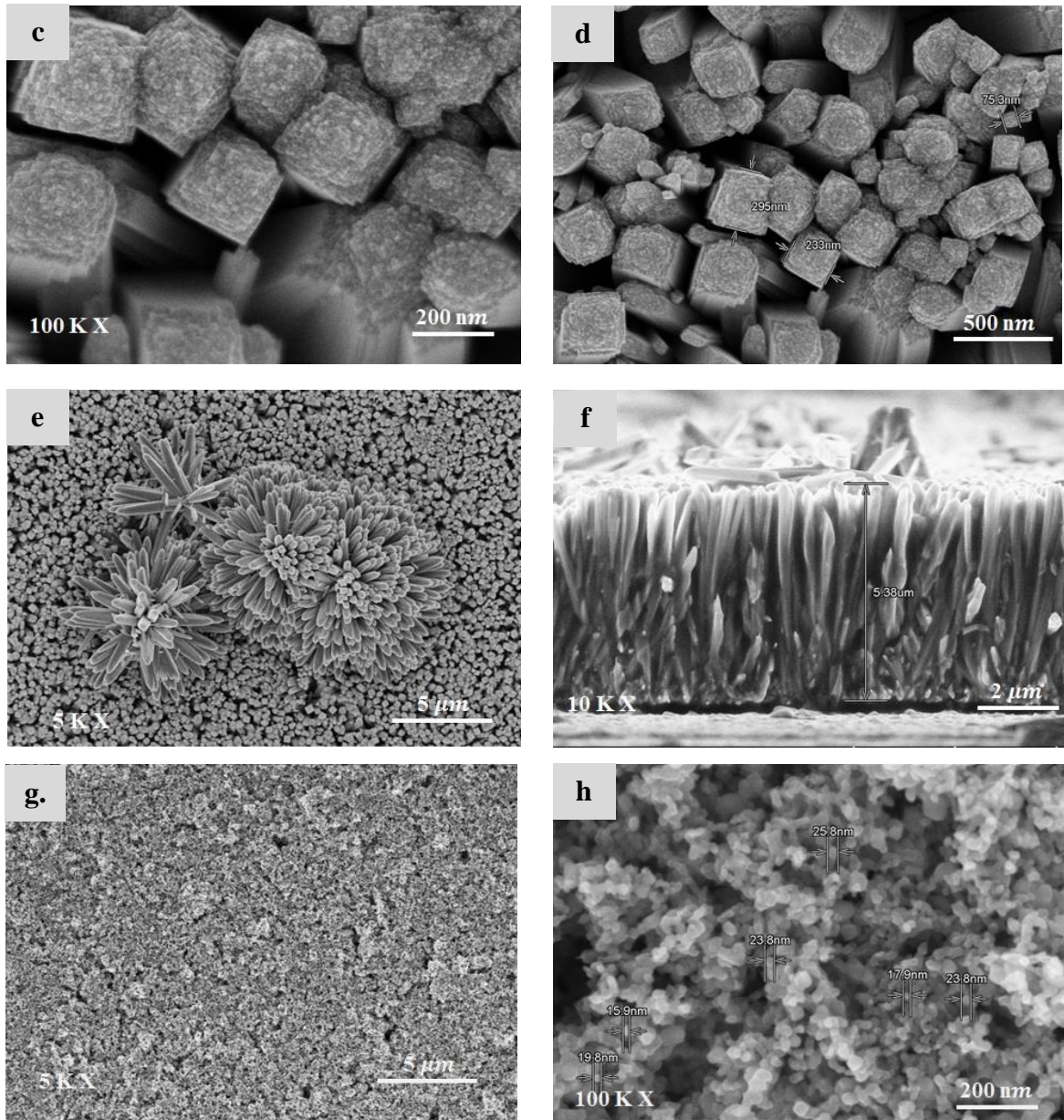
Figure 22. FESEM images of the top view of aligned TiO$_2$ nanorods (a)-(e), its cross section (f), and top view of TiO$_2$ nanoparticles (g)-(h).

The Raman spectra [Figure 23 (a)] were examined to compare the TC14-rGO, TC14-GO, and SDS-rGO film samples and to confirm the successful reduction of GO to rGO by using hydrazine hydrate. Two prominent peaks, namely, D and G bands, are found in the spectra of TC14-rGO and SDS-rGO samples. These bands are located in the range of 1367.8–1432.7 and 1582.7–1587.9 cm^{-1}, respectively. I_D/I_G ratio is necessary to predict the existence of defects and sizes in sp^2 domains [25]. The I_D/I_G ratio of TC14-rGO is 0.69, and this value is lower than that of SDS-rGO (I_D/I_G = 0.80). This result is attributed to the presence of rGO functionalization-assisted by triple tail surfactant and the

restoration of the sp^2 domain in the rGO structures after reduction is completed [26, 27]. An increase in the I_D/I_G ratio of SDS-rGO suggests that graphitic domains are distorted [28, 29] and rGO is exfoliated into a single-layer structure [30]. To calculate the number of layers of each rGO sample, we used the following equation: $\omega_G = 1581.6 + 11/(1 + n^{1.6})$ where ω_G is band position in wavenumbers and n is the number of layers present in the sample [31]. It is observed that the TC14-rGO and SDS-rGO samples contain approximately 2–4 layers and 5–6 layers, respectively, and these findings are consistent with those revealed through HRTEM.

(a)
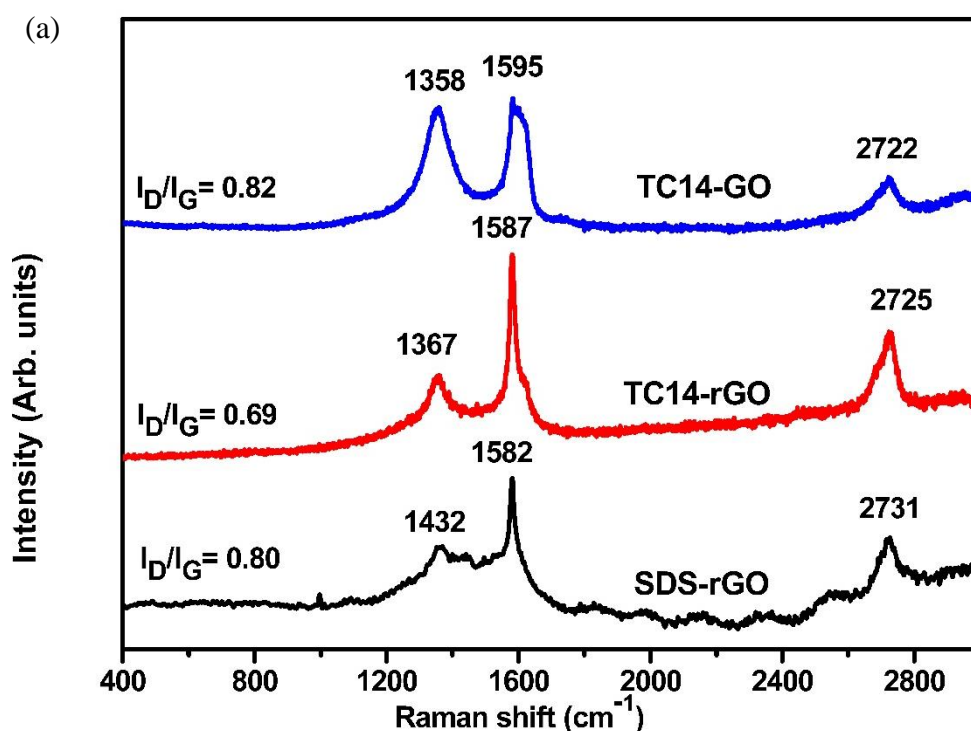
Figure 23. Micro-Raman spectra of TC14-rGO, SDS-rGO and TC14-GO sheets.

Micro-Raman spectra of TiO_2 nanorods reveals four peaks in the range of 100 to 800 cm^{-1} as shown in Figure 24 (a). The weak sharp band are observed at 121 cm^{-1}, while the broad band caused by the disordered lattice centered at 238 cm^{-1} related to two phonon scattering. Two intense peaks also observed at 446 and 612 cm^{-1} related to E_g and A_{1g} modes, respectively. The four peaks confirm the typical synthesized TiO_2 nanorods is in the rutile phase. Meanwhile, the micro-Raman spectrum of TiO_2 mixed-phase is shown in Figure 24 (b) which reveals seven peaks in the range of 100 to 800 cm^{-1}. The strongest band is at 144 cm^{-1} which related to E_g mode in anatase phase. Another peaks related to

anatase phase are at 198, 399, and 518 cm^{-1}. Two intense peaks at 448 and 611 cm^{-1} and broad band at 238 cm^{-1} confirms the rutile phase in the sample. This results confirms that the sample is in the mixed-phase.
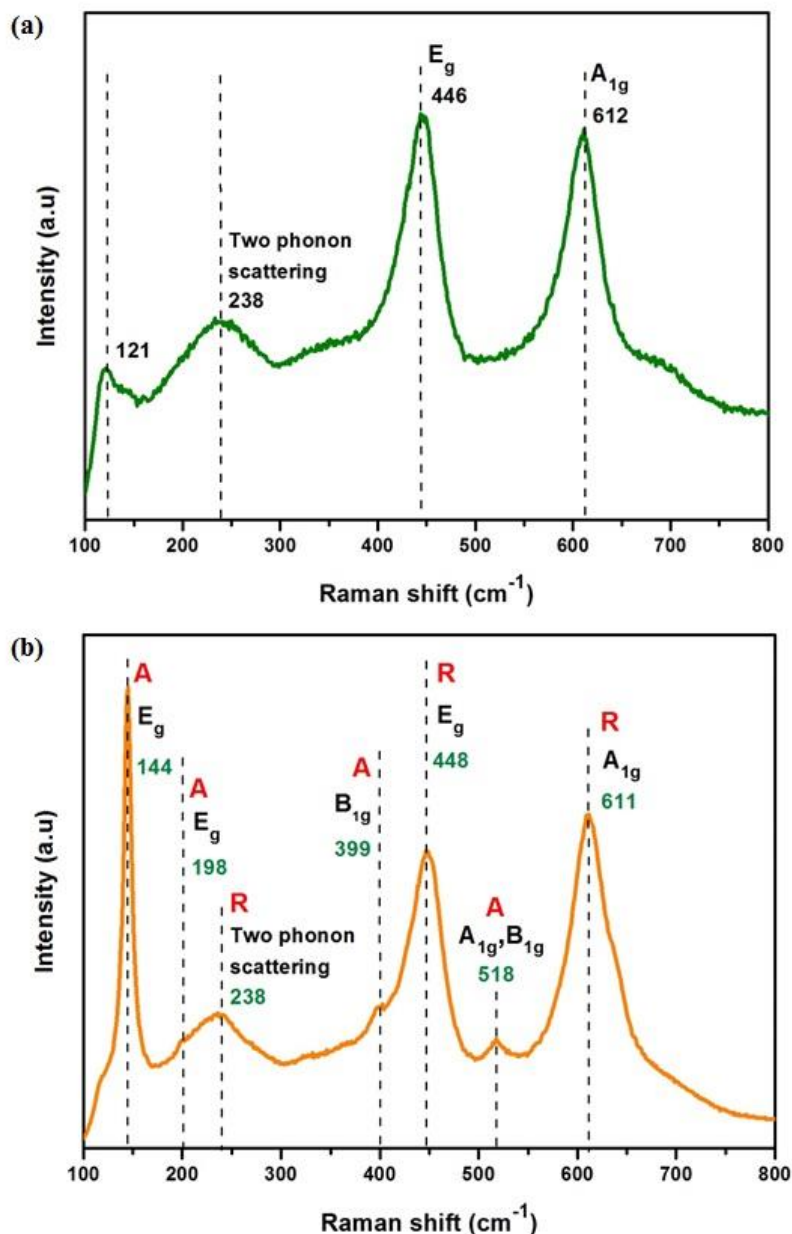
Figure 24. micro-Raman spectra of TiO$_2$ nanorods (a) and TiO$_2$ mixed-phase (b).

AFM was employed to confirm the thickness of TC14-rGO (Figure 25). The measured thickness of the rGO sheets is approximately 10–12 nm. This finding is consistent with the Raman result showing that the highest number of rGO layers is 10. The thickness of the rGO sheets is likely lower than that of pure GO because oxygen-containing functional groups and lattice defects are removed during chemical reduction. The AFM result also confirmed that the rGO sheets are

composed of thin and wrinkled sheets that helps to enhance the electrical, capacitance, optical, and optoelectronic properties.

(b)
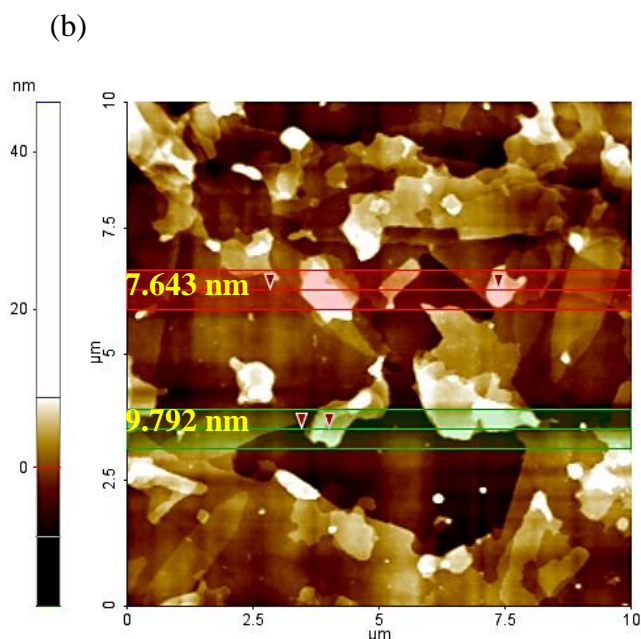
Figure 25. AFM of TC14-rGO sample.

The successful reduction of GO to rGO is also indicated by the transmittance values of the samples subjected to UV-vis analysis (Figure 26). The prepared rGO films maintain an optical transmittance of approximately 80–95% in the range of 500–800 nm. At a wavelength of less than 500 nm, the TC14-rGO sample yields the highest transparency rate of up to 80%, and this value is higher than that of SDS-rGO film (60%). An increase in the restacking number of layers and non-continuous rGO particles of the sample-assisted by SDS surfactant may contribute to the lower transmittance of the obtained film [10]. Another possible reason is the greater solubility promoted by TC14. When sprayed, the rGO sheets less likely form bundles, which subsequently form a more dispersed and cohesive film that enhances the traveling light. However, the TC14-GO electrode generates a slightly lower transmittance of (<85%) than TC14-rGO film does (~90%). The high transmittance values of TC14-rGO at above 550 nm are probably attributed to the low restacking of graphite structures after reduction and annealing occur and thus allow light to travel on FTO films [32]. This finding confirms that the oxygen-containing functional group in GO is reduced by hydrazine hydrate treatment. Thus, several layers of rGO sheets are produced. This result is consistent with that

described in a previous work revealing that the transmittance values increase as the number of layers decreases [10]. The transmittances of TC14-rGO, TC14-GO, and SDS-rGO films do not significantly alter the transparency of FTO substrates [32, 33].
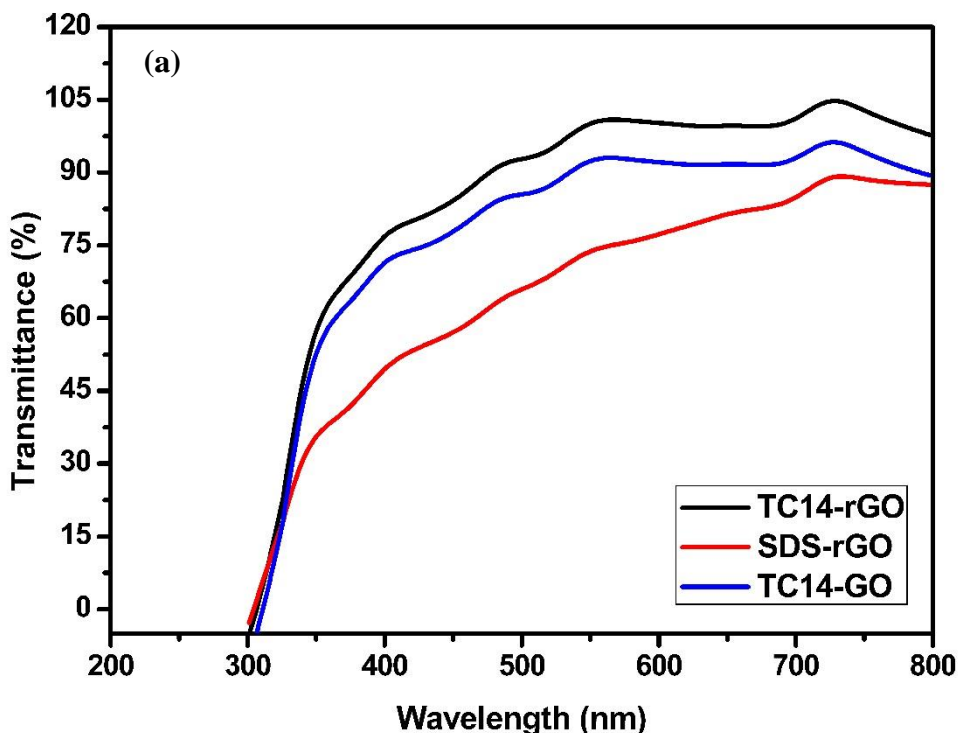
Figure 26. UV-Vis spectra of TC14-rGO, SDS-rGO and TC14-GO sheets.

The optical band gaps of TC14-rGO, TC14-GO, and SDS-rGO are determined on the basis of a Tauc plot (Figure 27). Single-layer graphene yields a zero-energy band gap [34]. However, oxidation through electrochemical exfoliation has increased the zero energy band gap of graphene layers to approximately 3.94 eV. This finding is possibly caused by the insertion of various oxygen-containing functional groups between graphite layers [35]. After GO is reduced, the energy band gap of TC14-rGO and SDS-rGO is decreased to approximately 3.92–3.98 eV. This result indicates that the elimination of several oxygen-containing functional groups partially reduces from GO structures [36]. However the SDS-rGO sample shows the highest energy band gap of 4.06-4.20 eV due to the low stabilized single-tail SDS surfactant on the rGO structures as compared to rGO assisted by triple-tails TC14. These results are supported by MicroRaman analysis that revealed a small decrease in the I_D/I_G ratio from 0.82 for GO to ~0.60–0.80 for

rGO samples; this decrease also corresponds to a slight decrease in defect density [36]. These observed band gaps in all of the samples indicate an intrinsic semiconductor.
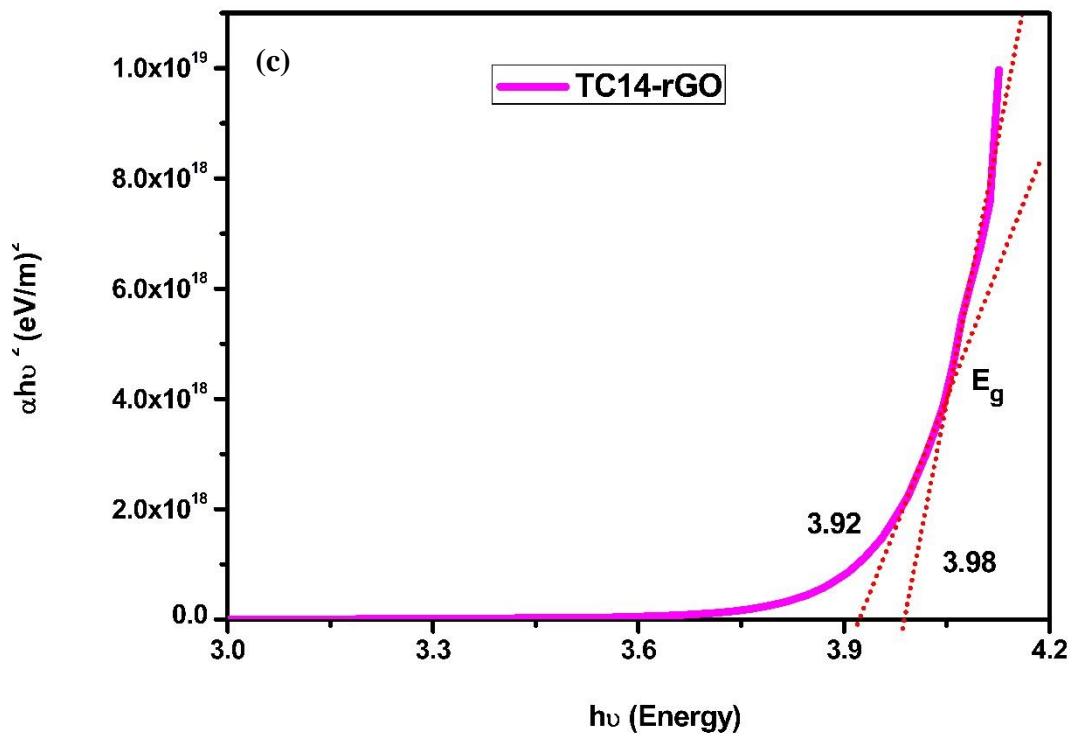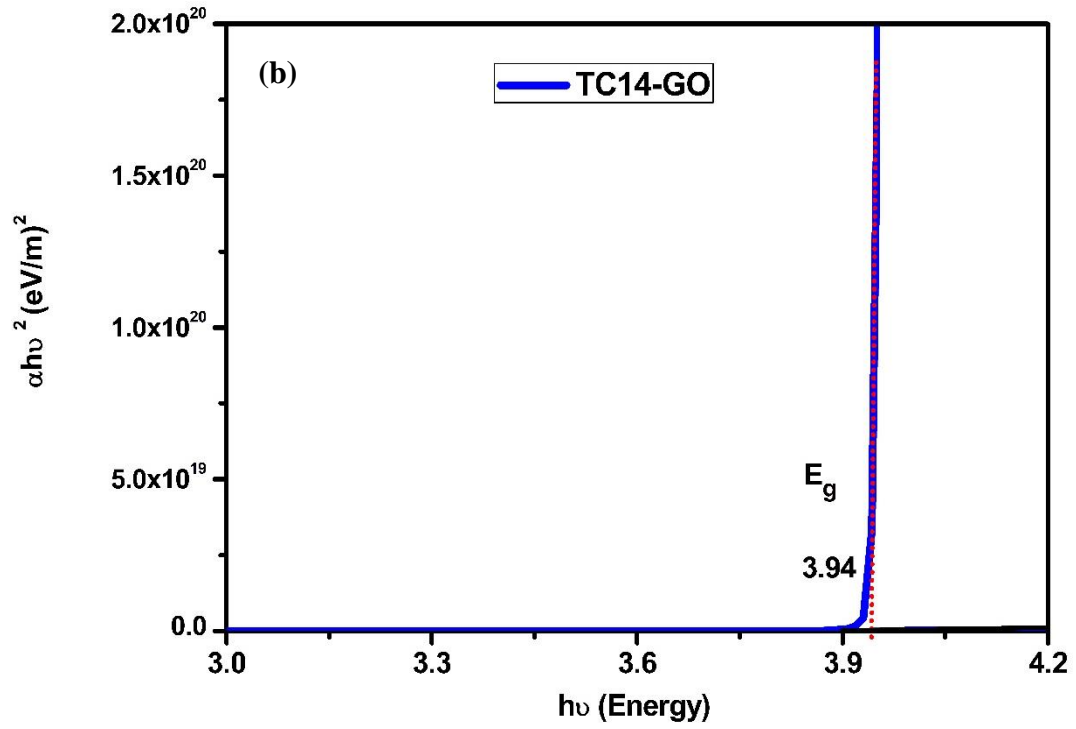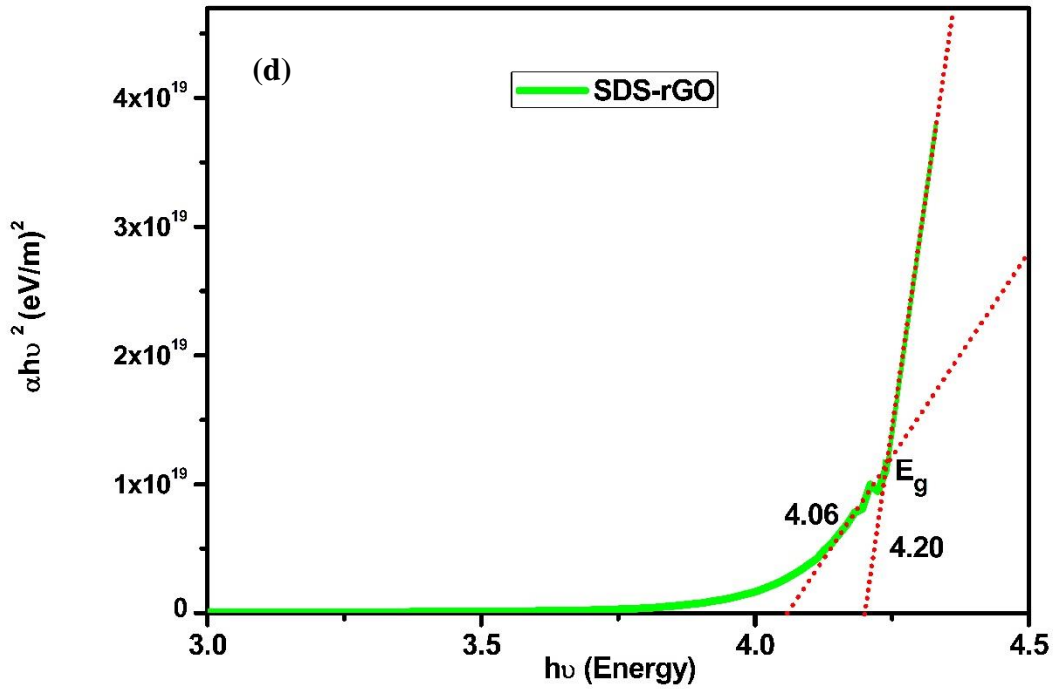
Figure 27. Energy band gaps of TC14-rGO, SDS-rGO and TC14-GO sheets.

Figure 28 compares the I–V curves of the TC14-rGO, TC14-GO, and SDS-rGO film samples. The TC14-rGO film exhibits the optimum I–V characteristics with the lowest resistance (R) of 3.0 Ω, followed by SDS-rGO with R of 3.4 Ω. By comparison, the TC14-GO film sample yields a slightly lower resistance (3.2 Ω) than the SDS-rGO sample does. This finding indicates that the use of TC14 plays a key role in stabilizing the graphitic sheets. Compared with SDS, TC14 facilitates an enhanced rGO dispersion during exfoliation that causes a higher conductive film after TC14 is transferred on the substrate [18, 23]. This result is consistent with that obtained in the MicroRaman analysis.
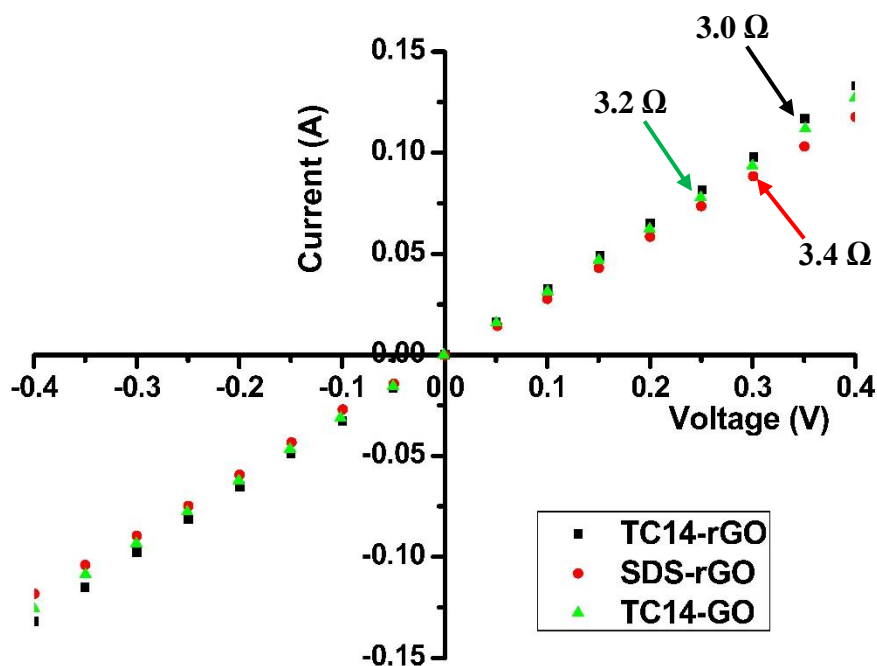
Figure 28. *I–V* curve of TC14-rGO, SDS-rGO and TC14-GO sheets.

Figure 29 illustrates the representative photocurrent density–voltage (*J–V*) curves of the DSSC with TiO_2 nanoparticles [19, 37] as a photoanode and TC14-rGO, TC14-GO, and SDS-rGO film samples as a CE. V_{OC} of the TC14-rGO film (0.65 V) is higher than that of SDS-rGO film (0.49 V). The recombination rate and interfacial resistance are decreased because of the incorporation of a TC14-rGO film [38]. J_{SC} of the TC14-rGO sample (2.72 mA cm^{-2}) is higher than that of SDS-rGO (2.35 mA cm^{-2}) because of the enhancement of electron collection and transport facilitated by a high-bridging system from the TC14 and rGO sheets to the FTO substrate [39]. This observation indicates that the rGO-assisted TC14 surfactant contains more stable rGO sheets, which then enhanced the diffusibility of the electrolyte in the DSSC [18, 23, 24]. The TC14-rGO film sample also yields a slightly higher FF (41.9) than the SDS-rGO film sample does (41.0). This finding is consistent with the lowest resistance observed in the TC14-rGO sample (3.0 Ω). The low resistance of the rGO-assisted TC14 is correlated with the morphological characteristics of the rGO structures. The higher surface area of the TC14-rGO sample provides easy pathways for electron movement and thus improves the FF of CE. These characteristics of DSSC indicate that the rGO-assisted TC14 can increase the interfacial contact and electron half-life and decrease the charge recombination rate via the rapid path for the transport of electrons to the FTO

glass [40]. By contrast, the rGO-assisted by SDS exhibits a slightly lower conversion efficiency (0.527%); this finding suggests that the sample contains a less affective area because of the single-tail-stabilized rGO on the FTO glass, which provides high surface resistance [24, 41]. However, the efficiency of 0.828% of the TC14-rGO in DSSC is lower than that described in a previous report because of different fabrication processes and raw materials [24]. Therefore, the TC14-rGO CE with a high catalytic activity and an excellent electrical conductivity is favourable for high-performance DSSC.

Sample	Voc (V)	Jsc (mA/cm²)	Fill Factor	Efficiency (%)
SDS-rGO	0.49	2.72	41.0	0.527
TC14-rGO	0.65	2.34	41.9	0.828
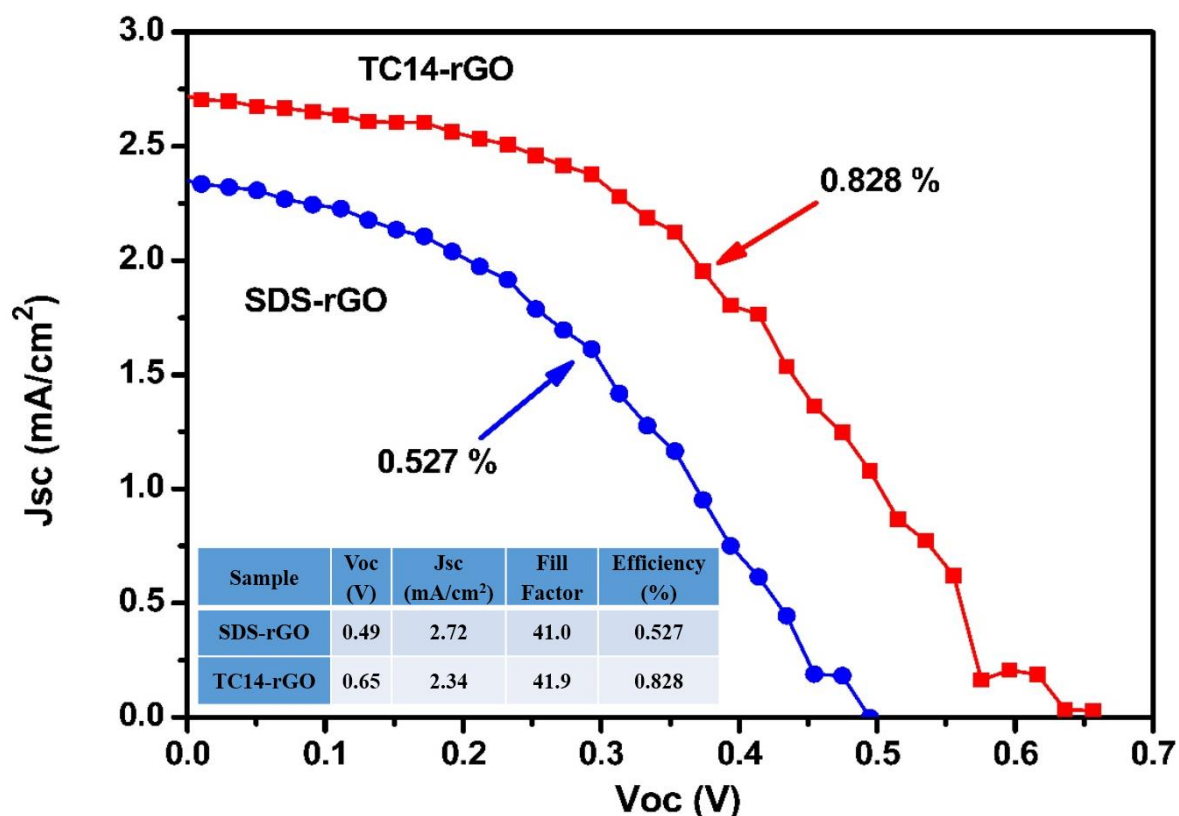
Figure 29. *J-V* curves obtained for the TC14-rGO and SDS-rGO modified CE based DSSCs under the illumination of simulated solar AM 1.5G irradiation

The possible reason for the improvement in the power conversion efficiency of TC14-rGO film in DSSC as follows. Reduction is performed on the basis of a typical reduction growth mechanism of GO to rGO using hydrazine hydrate [27]. In particular, TC14 reduces the surface tension of the rGO sheets. As a result, the dispersion of rGO on the FTO film surface is enhanced. Reduction also contributes to the enhancement of the dispersion of single- and multi-layers of rGO sheets. Therefore, the improvement of charge transfer resistance between rGO sheets and electrolyte is probably due to the removal of excess oxygen-containing

functional groups attached to the graphene sheets. The preheated rGO film samples also improve the structural properties of TC14-rGO sheets and the charge transfer between rGO sheets and electrolytes [42]. The low interaction between SDS and GO structures may produce few opening gaps and stacked layers. Thus, the highest resistance of the SDS-rGO film is obtained, as revealed by I–V measurement.

4.   Conclusion

We have built a facile and low-cost preparation method for the fabrication of counter electrode for DSSC using reduced graphene oxide assisted byTC14 surfactant. This highly active and stable TC14-rGO modified CE based DSSC showed improvement in the J_{SC}, V_{OC}, and FF functions. By comparison, the TC14-rGO film sample yields a higher solar efficiency (0.828%) than the SDS-rGO film sample (0.527%) does when TiO_2 nanoparticles are used in photoanode. This finding indicates that the usage of TC14 surfactant is an efficient stabilizer to enhance rGO dispersion and thus improve photovoltaic performance. Therefore, this work can be used as a basis for the development of a new generation of high-performance and low-cost DSSC and it offers a great exposure to the students to build their own solar cells.

5.   References

[1]   X. Xu, D. Huang, K. Cao, M. Wang, S.M. Zakeeruddin, M. Gratzel, Electrochemically reduced graphene oxide multilayer films as efficient counter electrode for dye-sensitized solar cells, Sci. reports (2013) 3.

[2]   Hagfeldt, G. Boschloo, L. Sun, L. Kloo, H. Pettersson, Dye-sensitized solar cells, Chem. Rev. 110(11) (2010) 6595-6663.

[3]   S. Thomas, T.G. Deepak, G.S. Anjusree, T.A. Arun, S.V. Nair, A.S. Nair, A review on counter electrode materials in dye-sensitized solar cells, J. Mater. Chem. A 2(13) (2014) 4474-4490.

[4]   M. Wu, X. Lin, Y. Wang, L. Wang, W. Guo, D. Qi, X. Peng, A. Hagfeldt, M. Gratzel, T. Ma, Economical Pt-free catalysts for counter electrodes of dye-sensitized solar cells, J. Amer. Chem. Soc. 134(7) (2012) 3419-3428.

[5]   S. Cho, S. H. Hwang, C. Kim, J. Jang, Polyaniline porous counter-electrodes for high performance dye-sensitized solar cells, J. Mater. Chem. 22(24) (2012) 12164-12171.

[6]   H. Xu, X. Zhang, C. Zhang, Z. Liu, X. Zhou, S. Pang, X. Chen, S. Dong, Z. Zhang, L. Zhang, Nanostructured titanium nitride/PEDOT: PSS composite films as counter electrodes of dye-sensitized solar cells, ACS Appl. Mater. Interf. 4(2) (2012) 1087-1092.

[7]   C.B. Jacobs, T.L. Vickrey, B.J. Venton, Functional groups modulate the sensitivity and electron transfer kinetics of neurochemicals at carbon nanotube modified microelectrodes. Analyst 136(17) (2011) 3557-3565.

[8]   A.A. Arbab, K.C. Sun, I.A. Sahito, A.A. Memon, Y.S. Choi, S.H. Jeong, Fabrication of textile fabric counter electrodes using activated charcoal doped multi walled carbon nanotube hybrids for dye sensitized solar cells, J. Mater. Chem. A 4(4) (2016) 1495-1505.

[9]   H. Hoshi, S. Tanaka, T. Miyoshi, Pt-graphene electrodes for dye-sensitized solar cells, Mater. Sci, Eng., B, 190, (2014) 47–51.

[10]   B. Tripathi, P. Yadav, K. Pandey, P. Kanade, M. Kumar, M. Kumar, Investigating the role of graphene in the photovoltaic performance improvement of dye-sensitized solar cell, Mater. Sci, Eng., B, 190, (2014) 111–118.

[11]   J.N. Coleman, Liquid exfoliation of defect-free graphene, Acc. Chem. Res. 46(1) (2013) 14-22.

[12]   A. Kaniyoor, and S. Ramaprabhu, Soft functionalization of graphene for enhanced tri-iodide reduction in dye sensitized solar cells, J. Mater. Chem. 22(17) (2012) 8377-8384.

[13]   L. Qiu, H. Zhang, W. Wang, Y. Chen, R. Wang, Effects of hydrazine hydrate treatment on the performance of reduced graphene oxide film as counter electrode in dye-sensitized solar cells, Appl. Surf. Sci. 319 (2014) 339-343.

[14]   J. Velten, A.J., Mozer, D. Li, D. Officer, G. Wallace, R. Baughman, A. Zakhidov, Carbon nanotube/graphene nanocomposite as efficient counter electrodes in dye-sensitized solar cells. Nanotechnol. 23(8) (2012) 085201.

[15]   C. Xu, J. Li, X. Wang, J. Wang, L. Wan, Y. Li, M. Zhang, X. Shang, Y. Yang. Synthesis of hemin functionalized graphene and its application as a counter electrode in dye-sensitized solar cells, Mater. Chem. Phys. 132(2) (2012) 858-864.

[16] D. Dodoo-Arhin, R.C.T. Howe, G. Hu, Y. Zhang, P. Hiralal, A. Bello, A. Bello, G. Amaratunga, T. Hasan, Inkjet-printed graphene electrodes for dye-sensitized solar cells. Carbon 105 (2016) 33-41.

[17] Q. Zhang, Y. Liu, Y. Duan, N. Fu, Q. Liu, Y. Fang, Q. Sun, Y. Lin, Mn_3O_4/graphene composite as counter electrode in dye-sensitized solar cells, RSC Adv. 4(29) (2014) 15091-15097.

[18] A. Jena, S.P. Mohanty, P. Kumar, J. Naduvath, V. Gondane, P. Lekha, J. Das, H.K. Narula, S. Mallick, P. Bhargava, Dye sensitized solar cells: a review. Transactions of the Indian Ceram. Soc. 71(1) (2012) 1-16.

[19] A.B. Suriani, M.D. Nurhafizah, A. Mohamed, I. Zainol, A.K. Masrom, A facile one-step method for graphene oxide/natural rubber latex nanocomposite production for supercapacitor applications, Mater. Lett. 161 (2015) 665-668.

[20] A.B. Suriani, M.D. Nurhafizah, A. Mohamed, A.K. Masrom, V. Sahajwalla, R.K. Joshi, Highly conductive electrodes of graphene oxide/natural rubber latex-based electrodes by using a hyper-branched surfactant, Mater. & Des. 99 (2016) 174-181.

[21] E.S. Kwak, W. Lee, N.G. Park, J. Kim, H. Lee, Compact Inverse-opal electrode using non-aggregated TiO_2 nanoparticles for dye-sensitized solar cells, Adv. Funct. Mater. 19(7) (2009) 1093-1099.

[22] F. Barroso-Bujans, S. Cerveny, R. Verdejo, J.J. del Val, A. Alegra, J. Colmenero, Permanent adsorption of organic solvents in graphite oxide and its effect on the thermal exfoliation, Carbon 48(4) (2010) 1079-1087.

[23] B. Tripathi, P. Yadav, K. Pandey, P. Kanade, M. Kumar, M. Kumar, Investigating the role of graphene in the photovoltaic performance improvement of dye-sensitized solar cell, Mater. Sci. Eng., B 190 (2014) 111-118.

[24] Y. Li, H. Wang, Q. Feng, G. Zhou, Z-S. Wang, Reduced Graphene Oxide-TaON Composite As a High-Performance Counter Electrode for Co (bpy) 33+/2+-Mediated Dye-Sensitized Solar Cells, ACS Appl. Mater. & Interf. 5(16) (2013) 8217-8224.

[25] A. Mohamed, A.K. Anas, A.B. Suriani, A. Azira, M. Sagiska, P. Brown, J. Eastoe, A. Kamari, N.H. Hashim, I.M. Isa, Preparation of multiwall carbon nanotubes (MWCNTs) stabilised by highly branched hydrocarbon surfactants and dispersed in natural rubber latex nanocomposites. Colloid Polym. Sci. 292(11) (2014) 3013-3023.

[26] J. Fan, S. Liu, J. Yu, Enhanced photovoltaic performance of dye-sensitized solar cells based on TiO 2 nanosheets/graphene composite films, J. Mater. Chem. 22(33) (2012) 17027-17036.

[27] F. Tuinstra and J.L. Koenig, Raman spectrum of graphite, J. Chem. Phys. 53(3) (1970) 1126-1130.

[28] Q. Xiang, J. Yu, M. Jaroniec, Preparation and enhanced visible-light photo catalytic H_2-production activity of graphene/C3N4 composites, J. Phys. Chem. C 115(15) (2011) 7355-7363.

[29] S. Stankovich, D.A. Dikin, R.D. Piner, K.A. Kohlhaas, A. Kleinhammes, Y. Jia, Y. Wu, S.T. Nguyen, R.S. Ruoff, Synthesis of graphene-based nanosheets via chemical reduction of exfoliated graphite oxide, Carbon 45(7) (2007) 1558-1565.

[30] M. Ghislandi, E. Tkalya, A. Alekseev, C. Koning, G. De With, Electrical conductive behaviour of polymer composites prepared with aqueous graphene dispersions, Appl. Mater. Today 1(2) (2015) 88-94.

[31] L.C. Sim, K.H. Leong, S. Ibrahim, P. Saravanan, Graphene oxide and Ag engulfed TiO_2 nanotube arrays for enhanced electron mobility and visible-light-driven photocatalytic performance, J. Mater. Chem. A 2(15) (2014) 5315-5322.

[32] C.-H. Tsai, C.-H. Chen, Y.-CY. Hsiao, P.-Y. Chuang, Investigation of graphene nanosheets as counter electrodes for efficient dye-sensitized solar cells, Org. Electron. 17 (2015) 57-65.

[33] M. Wall, The Raman spectroscopy of graphene and the determination of layer thickness, (2011). Thermo Scientific, [Enligne]. Available: https://tools.thermofisher.com/content/sfs/brochures/AN52252_E%201111%20LayerThkns_H_1.pdf

[34] R. Cruz, D.A.P. Tanaka, A. Mendes, Reduced graphene oxide films as transparent counter-electrodes for dye-sensitized solar cells, Sol. Energy 86(2) (2012) 716-724.

[35] H.-S. Jang, J.-M. Yun, D.-Y. Kim, D.-W. Park, S.-I., Na, S.-S., Kim, Moderately reduced graphene oxide as transparent counter electrodes for dye-sensitized solar cells, Electrochim. Acta 81 (2012) 301-307.

[36] Z.-Y. Li, M.S. Akhtar, J.H. Kuk, B.-S. Kong, O.B. Yang, Graphene application as a counter electrode material for dye-sensitized solar cell, Mater. Lett. 86 (2012) 96-99.

[37] M.S. Poorali and M.M. Bagheri-Mohagheghi, Comparison of chemical and physical reduction methods to prepare layered graphene by graphene oxide: optimization of the structural properties and tuning of energy band gap, J. Mater. Sci: Mater. Electron. 27(1) (2016) 260-271.

[38] H.C. Hsu, I. Shown, H.Y. Wei, Y.C. Chang, H.Y. Du, Y.C. Chang, et al., Graphene oxide as a promising photocatalyst for CO_2 to methanol conversion, Nanoscale 5(1) (2013) 262-268.

[39] M.K. Ahmad, V. M. Mohan, K. Murakami, Hydrothermal growth of bilayered rutile-phased TiO2 nanorods/micro-size TiO2 flower in highly acidic solution for dye-sensitized solar cell, J. Sol-Gel Sci. Technol. 73(3) (2015) 655-659.

[40] G.S. Han, S. Lee, E.S. Yu, S.P. Park, I.S. Cho, H.S. Jung,mEpitaxial anatase TiO_2 nanorods array with reduced interfacial charge recombination for solar water splitting. J. Electrochem. Soc. 163(6) (2016) 469-473.

[41] Y.B. Tang, C.S. Lee, J. Xu, Z.T. Liu, Z.H. Chen, Z. He, Y.L. Cao, et al., Incorporation of graphene in nanostructured TiO_2 films via molecular grafting for dye-sensitized solar cell application. ACS Nano 4(6) (2010) 3482-3488.

[42] M. Motlak, N.A.M. Barakat, M.S. Akhtar, A.M. Hamza, A. Yousef, H. Fouad, O.B. Yang, Influence of GO incorporation in TiO_2 nanofibers on the electrode efficiency in dye-sensitized solar cells, Ceram. Int. 41(1) (2015) 1205-1212.

[43] H. Wang, S.L. Leonard, Y.H. Hu, Promoting effect of graphene on dye-sensitized solar cells, Ind. Eng. Chem. Res. 51(32) (2012) 10613-10620.

[44] H. Choi, H. Kim, S. Hwang, Y. Han, M. Jeon, Graphene counter electrodes for dye-sensitized solar cells prepared by electrophoretic deposition, J. Mater. Chem. 21(21) (2011) 7548-7551.